Production for Cosmic Ray Physics in the Atmosphere

1. Cosmic ray spectra and composition: open questions
2. QCD predictions and experimental data
3. Uncertainties and their impact on atmospheric neutrino flux
4. Input for Monte Carlo generators for air shower physics

based on work by Garzelli, Moch, Sigl

DFG Deutsche Forschungsgemeinschaft

PROJEKTTRÄGER FÜR DAS Bundesministerium für Bildung und Forschung

UHH Universität Hamburg
DER FORSCHUNG | DER LEHRE | DER BILDUNG

Günter Sigl
II. Institut theoretische Physik, Universität Hamburg

The All Particle Cosmic Ray Spectrum

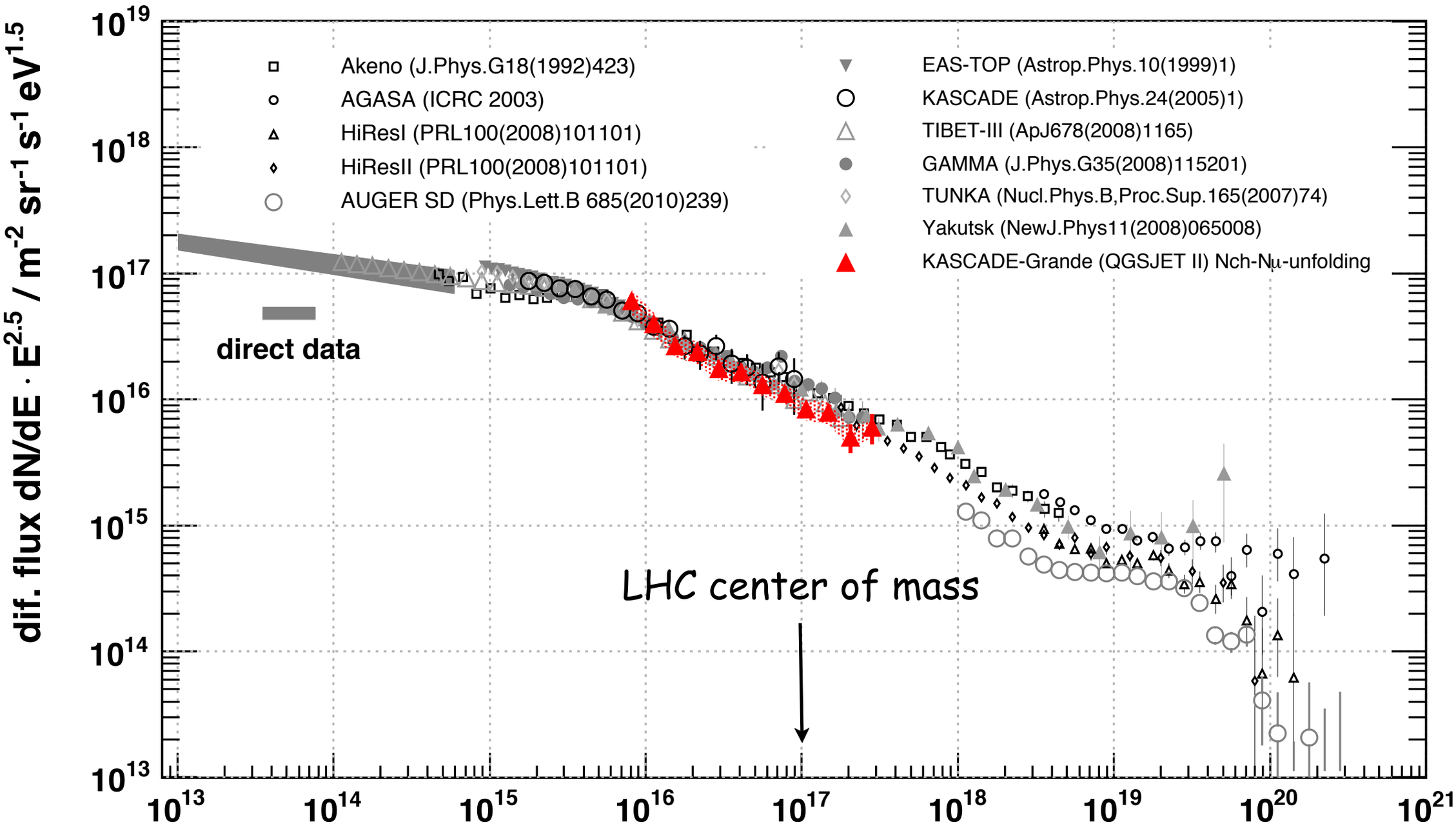

KASCADE-Grande collaboration, arXiv:1111.5436

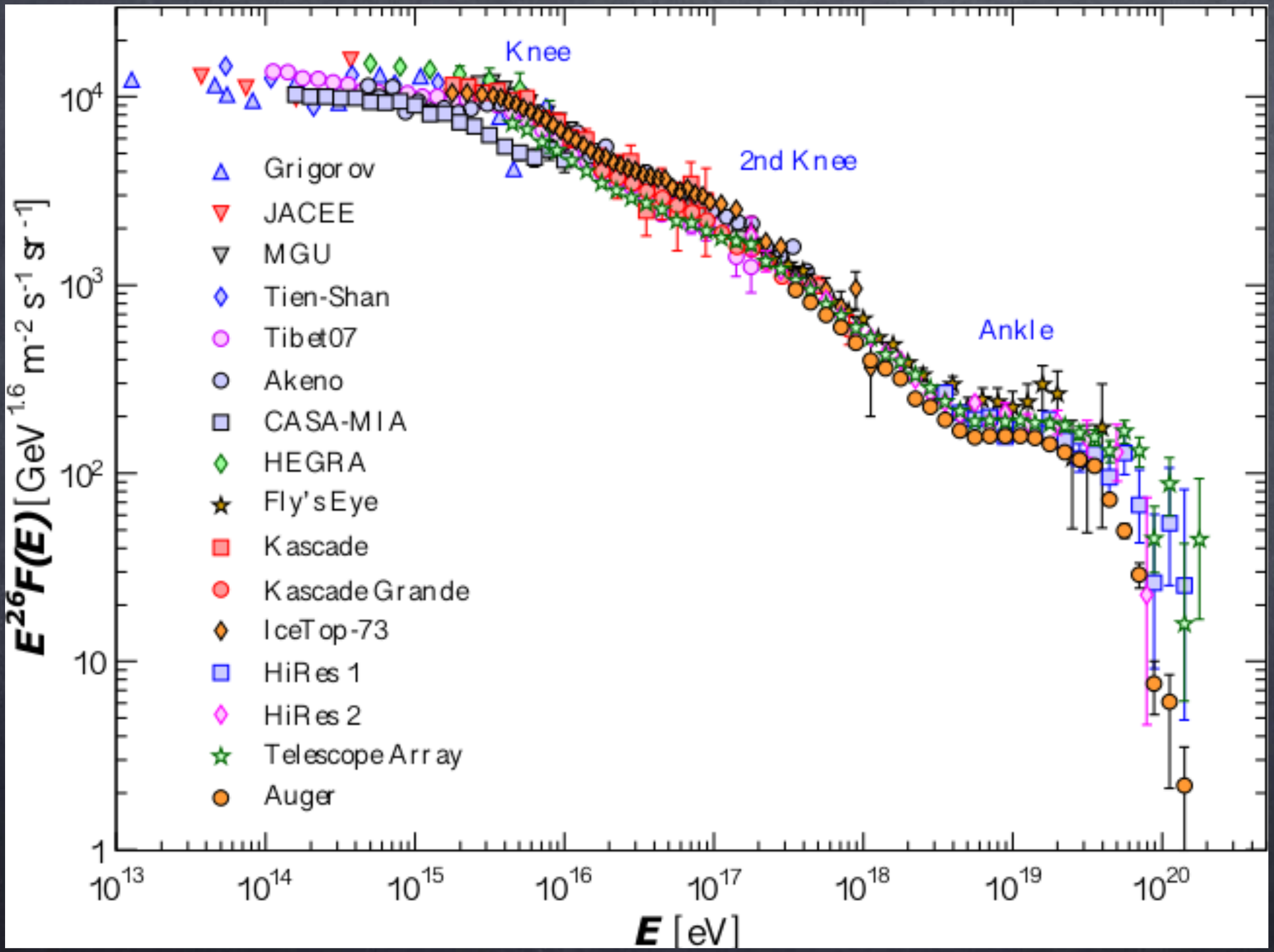
Knee
2nd Knee
Ankle
Grigorov
JACEE
MGU
Tien-Shan
Tibet07
Akeno
CASA-MIA
HEGRA
Fly's Eye
Kascade
Kascade Grande
IceTop-73
HiRes 1
HiRes 2
Telescope Array
Auger
$E^{2.6}F(E)$ [GeV$^{1.6}$ m^{-2} s^{-1} sr^{-1}]
E [eV]
10^4
10^3
10^2
10
1
10^{13}
10^{14}
10^{15}
10^{16}
10^{17}
10^{18}
10^{19}
10^{20}

Atmospheric Showers and their Detection

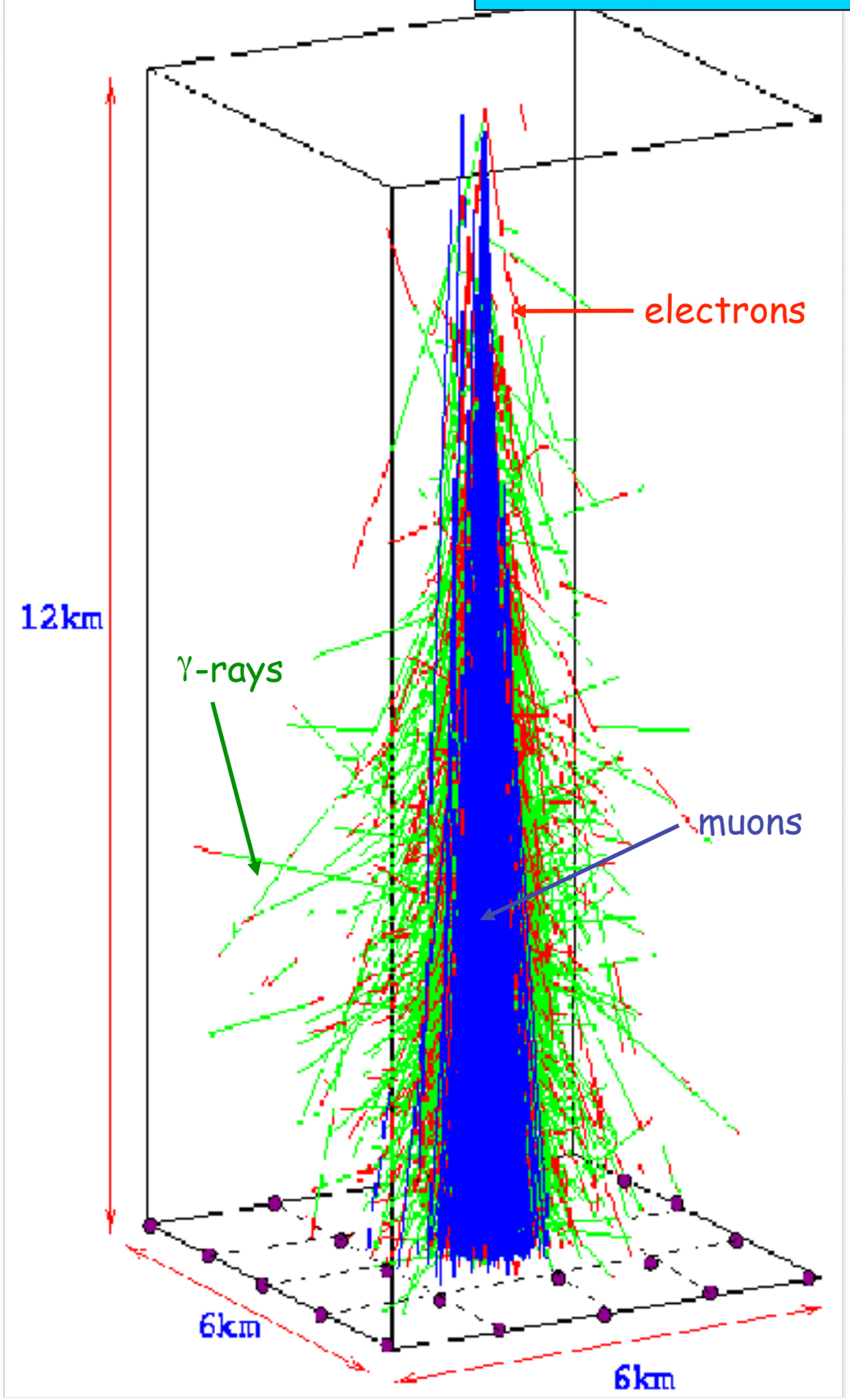

Fly's Eye technique measures fluorescence emission

The shower maximum is given by

$$X_{max} \sim X_0 + X_1 \log E_p$$

where X_0 depends on primary type for given energy E_p

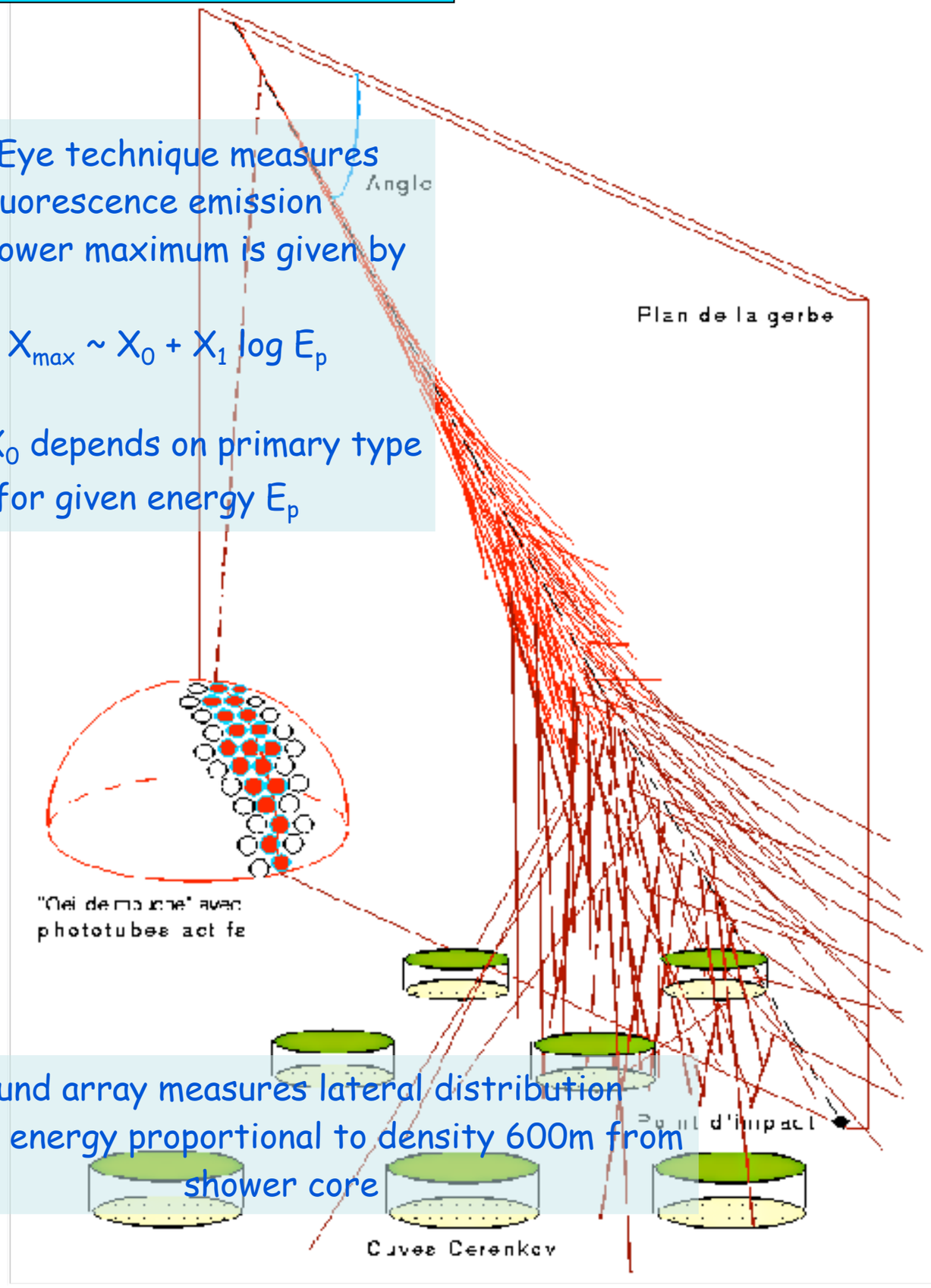

Ground array measures lateral distribution

Primary energy proportional to density 600m from shower core

Pierre Auger Spectra

Auger exposure = 50000 km^2 sr yr, 102901 events above 3x10^{18} eV until end 2014

Pierre Auger Collaboration, PRL 101, 061101 (2008)
and Phys.Lett.B 685 (2010) 239
ICRC 2015, arXiv:1509.03732

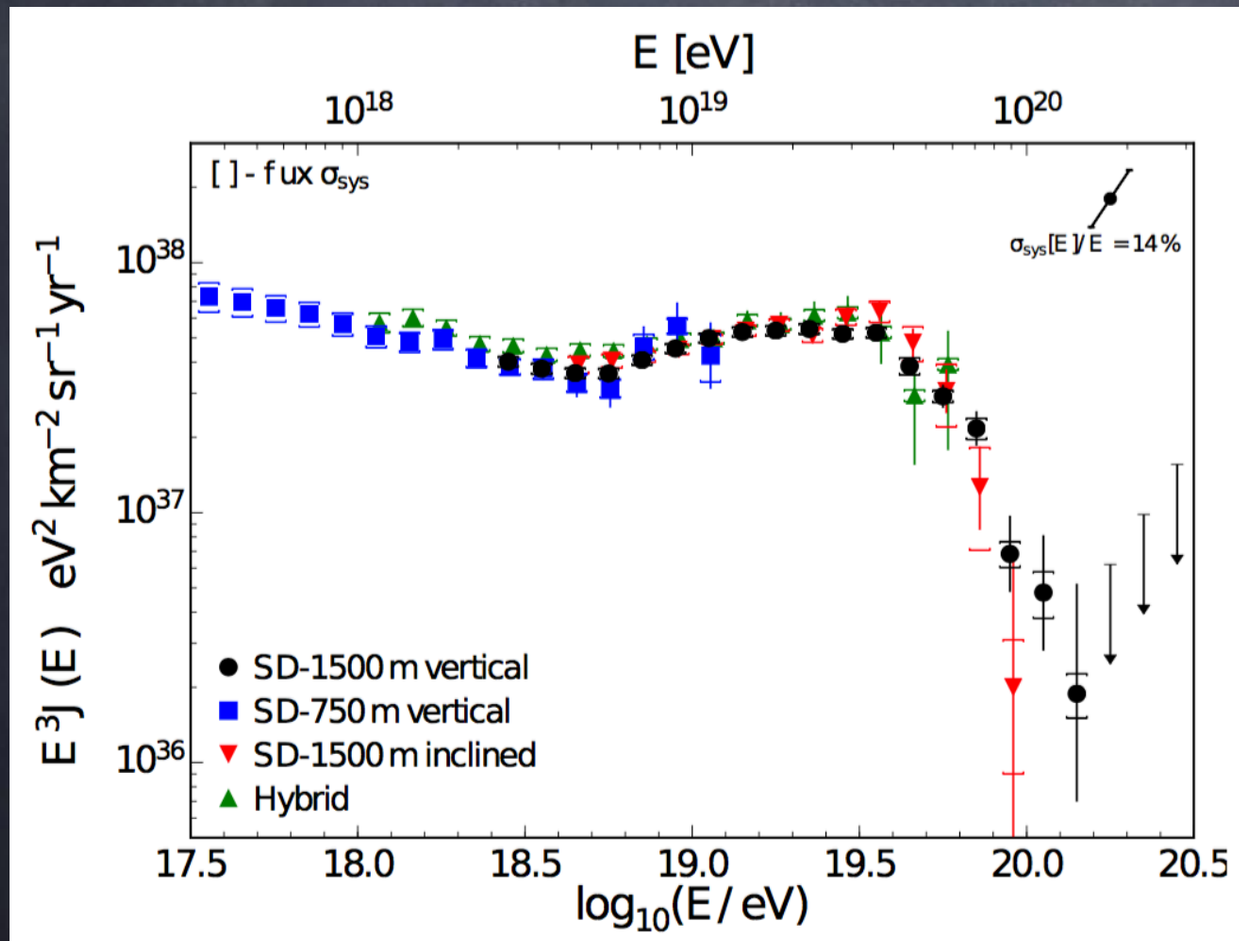

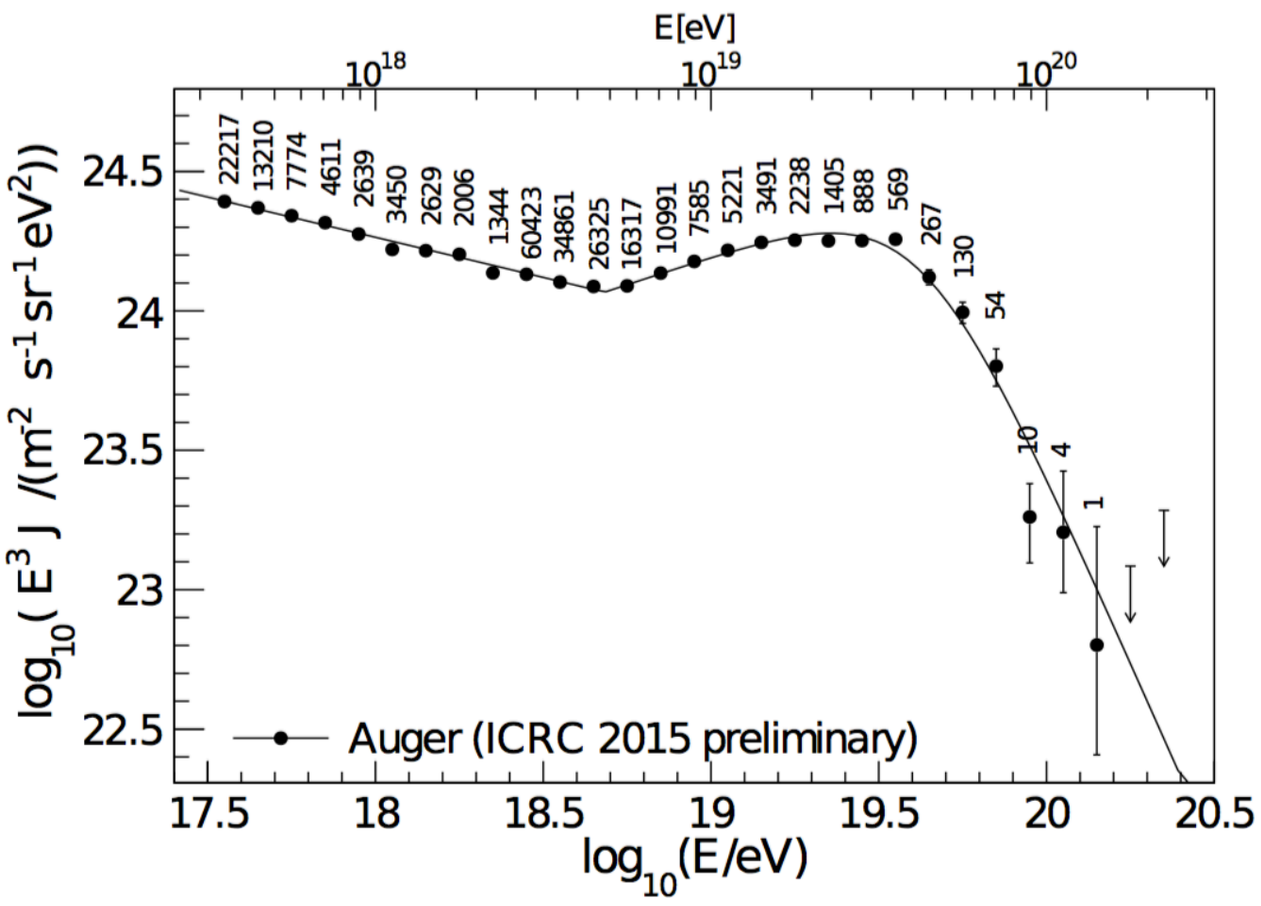

Mass Composition

Depth of shower maximum X_{max} and its distribution (measured by fluorescence detectors) and muon content (measured by ground detectors) contain information on primary mass composition

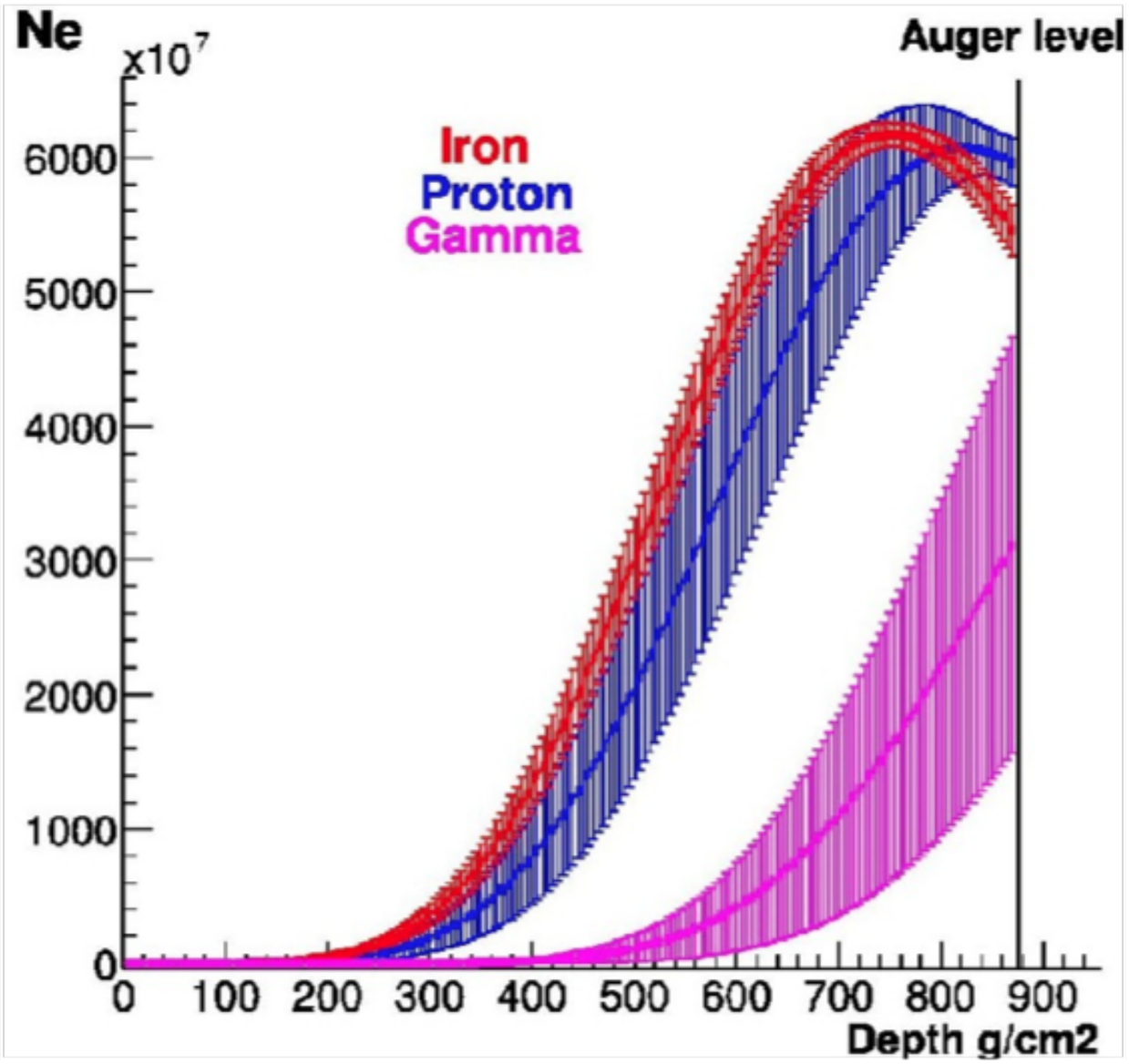

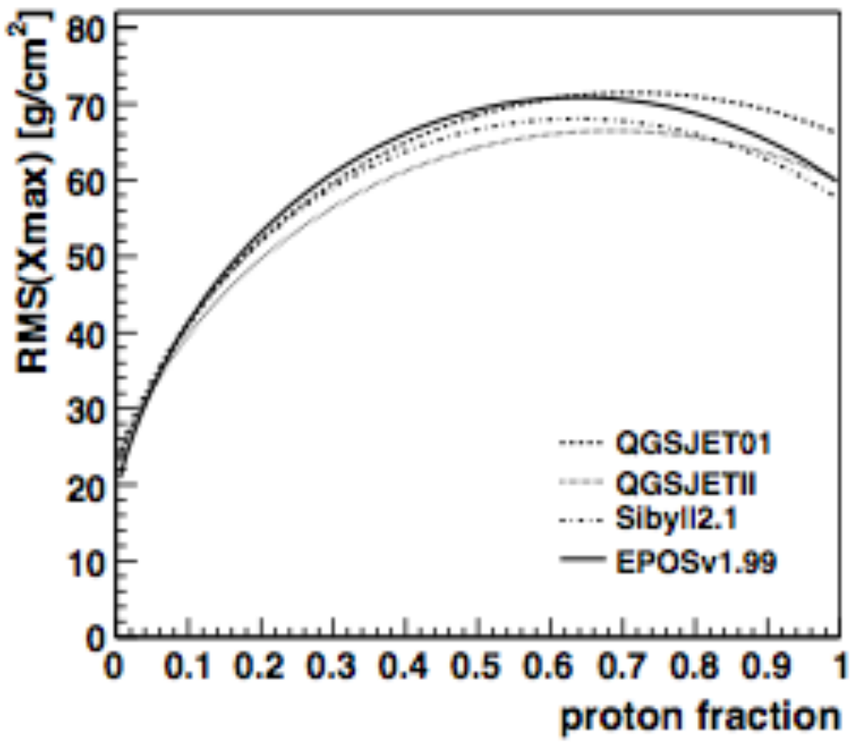

FIGURE 1. RMS($X_{\max}$) from different hadronic interaction models [23] and a two-component p/Fe composition model ($E = 10^{18}$ eV).

Pierre Auger data suggest a heavier composition toward highest energies:

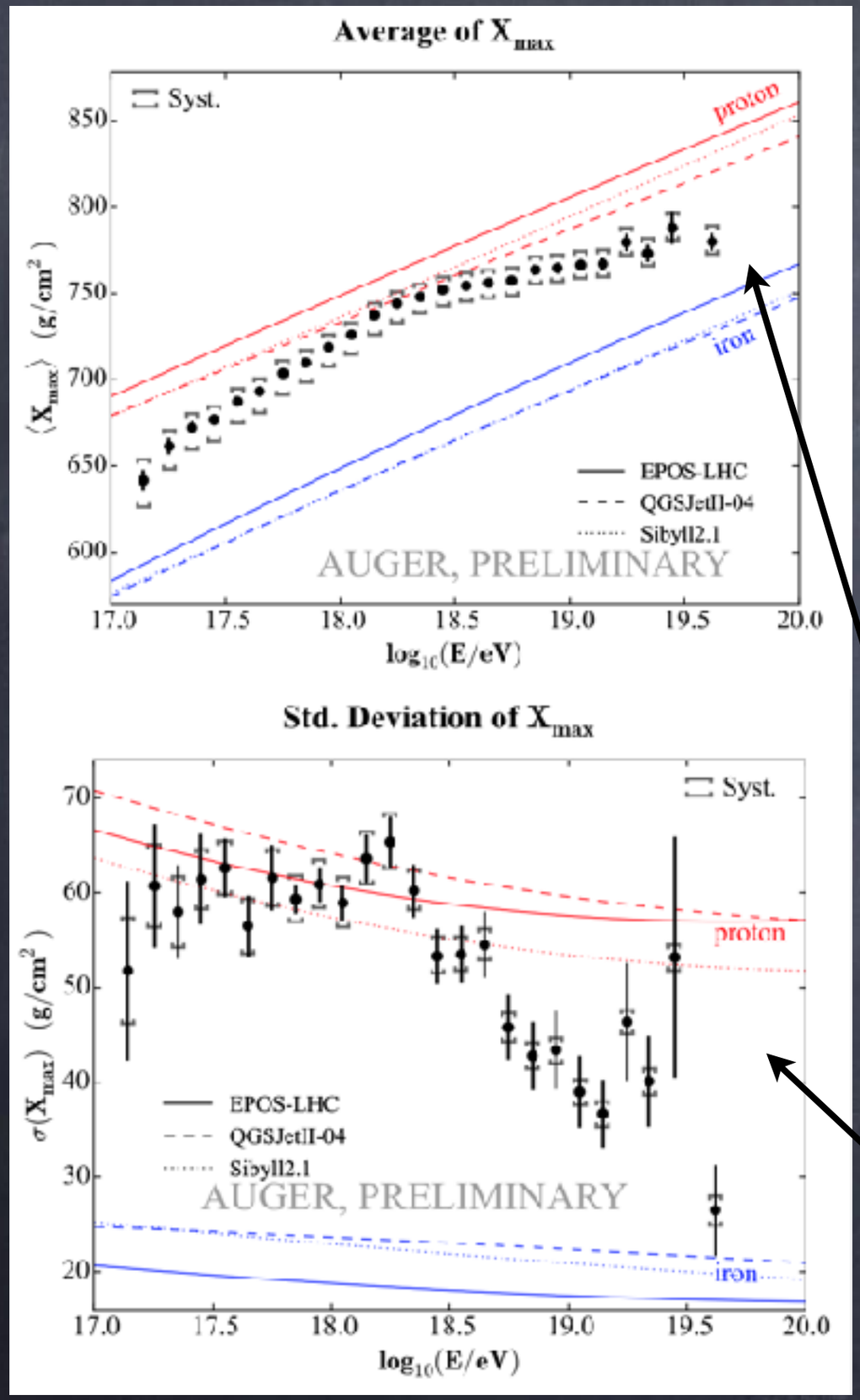

Pierre Auger Collaboration, arXiv:1509.03732

but not confirmed on the northern hemisphere by HiRes and Telescope Array which are consistent with protons

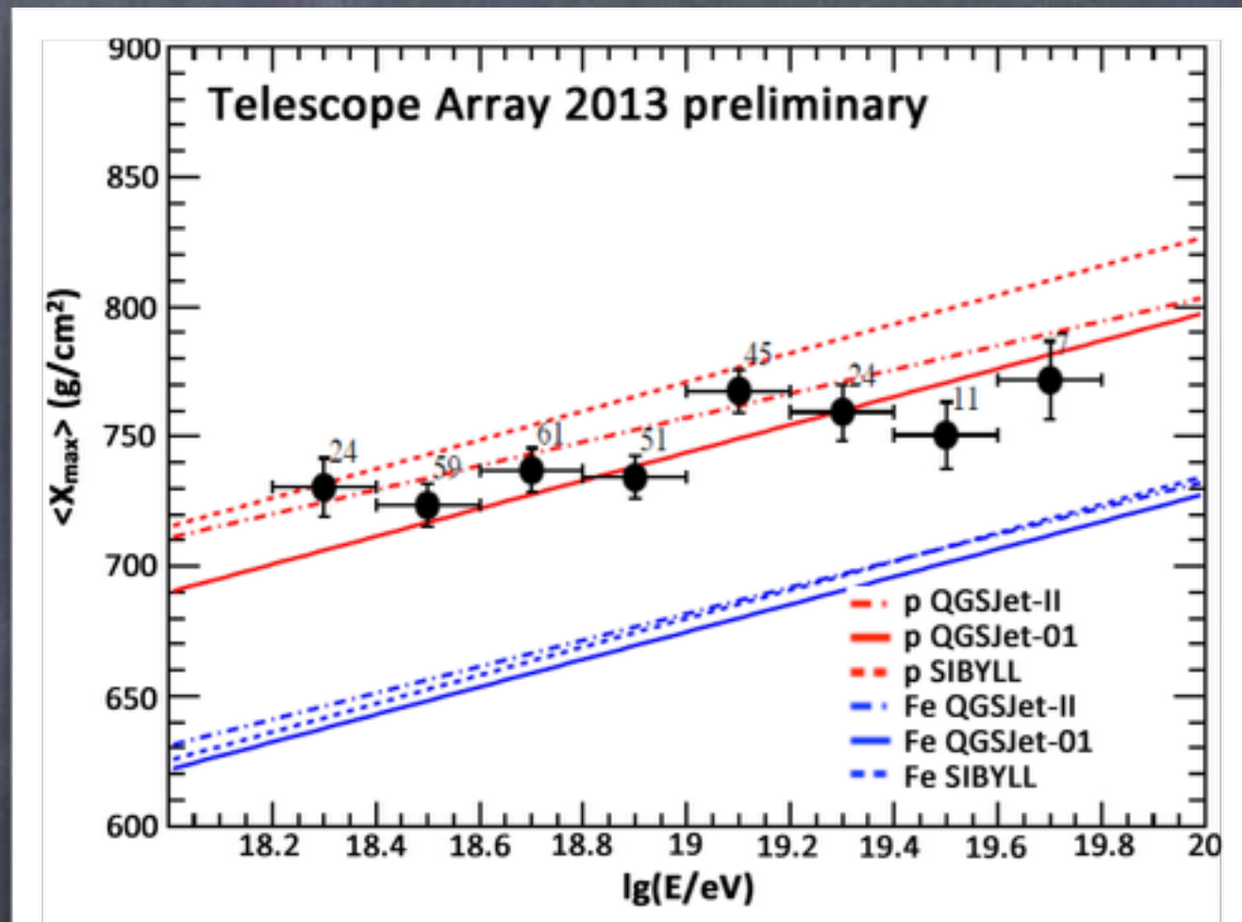

potential tension with air shower simulations and some hadronic interaction models because a mixed composition would predict larger RMS(X_{max})

combined measurement of X_{max} and its fluctuation $\sigma(X_{max})$ can be translated to distribution of atomic mass *A* **within a given hadronic interaction model**

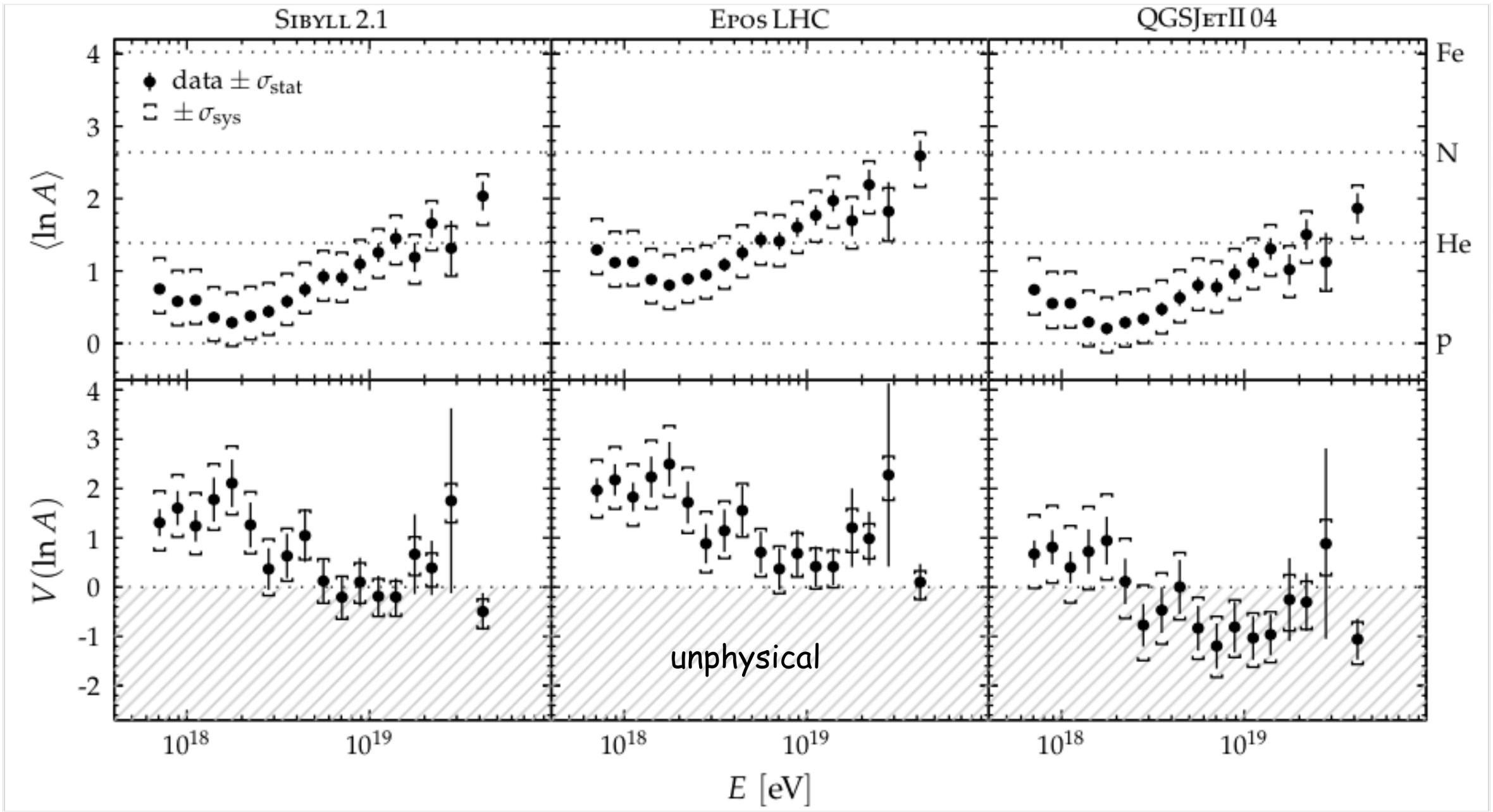

Pierre Auger Collaboration, arXiv:1409.4809

would imply that fluctuations predicted by a pure composition already higher than observed

An attempt to reconstruct individual elements

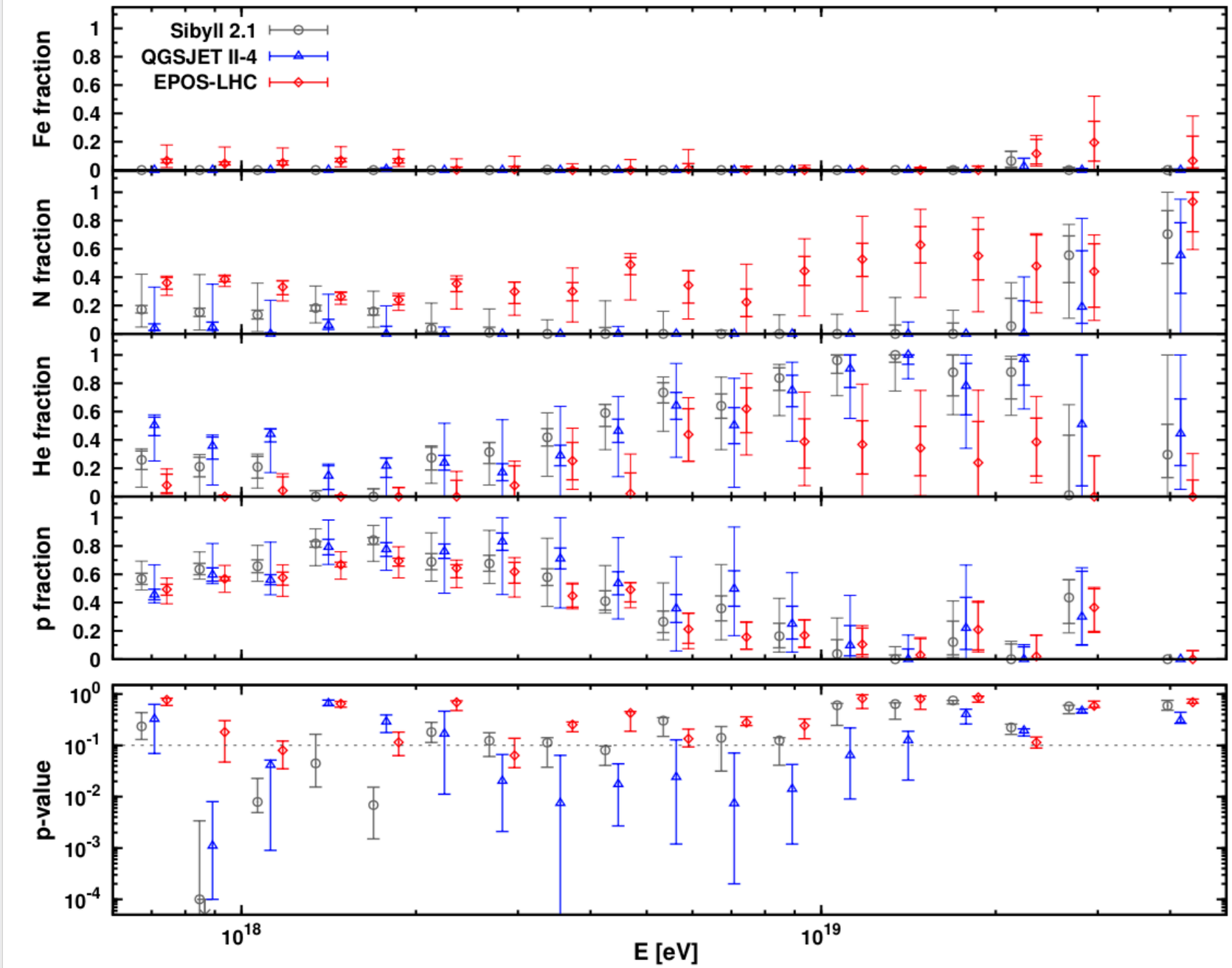

FIG. 4: Fitted fraction and quality for the scenario of a complex mixture of protons, helium nuclei, nitrogen nuclei, and iron nuclei. The upper panels show the species fractions and the lower panel shows the p-values.

Pierre Auger Collaboration, arXiv:1409.5083

Muon number measured at 1000 m from shower core systematically higher than predicted

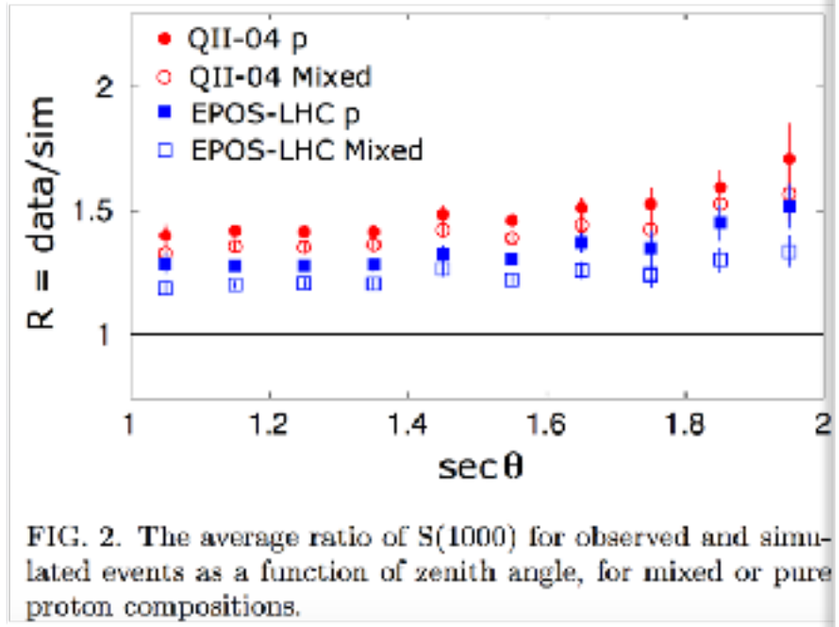

FIG. 2. The average ratio of S(1000) for observed and simulated events as a function of zenith angle, for mixed or pure proton compositions.

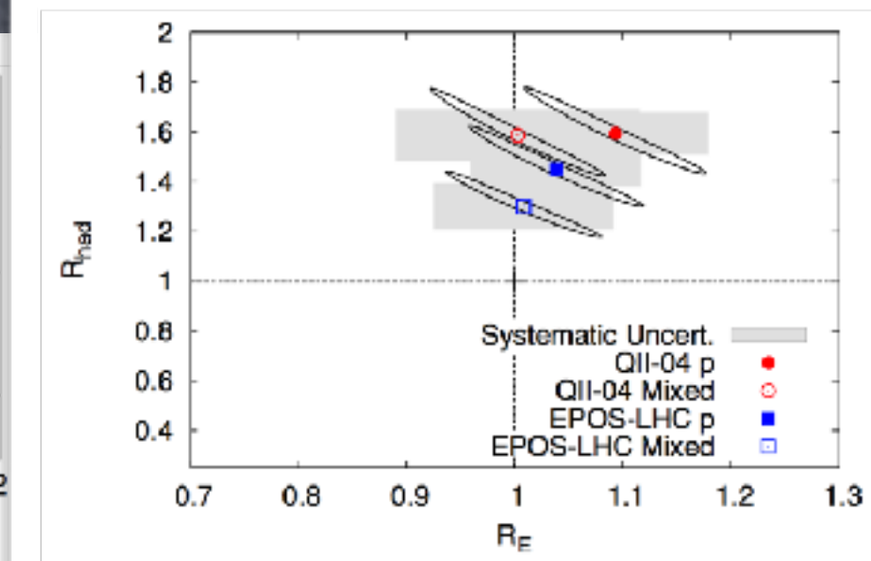

FIG. 4. Best-fit values of R_E and $R_{\rm had}$ for QGSJet-II-04 and EPOS-LHC, for pure proton (solid circle/square) and mixed composition (open circle/square). The ellipses and gray boxes show the 1-σ statistical and systematic uncertainties.

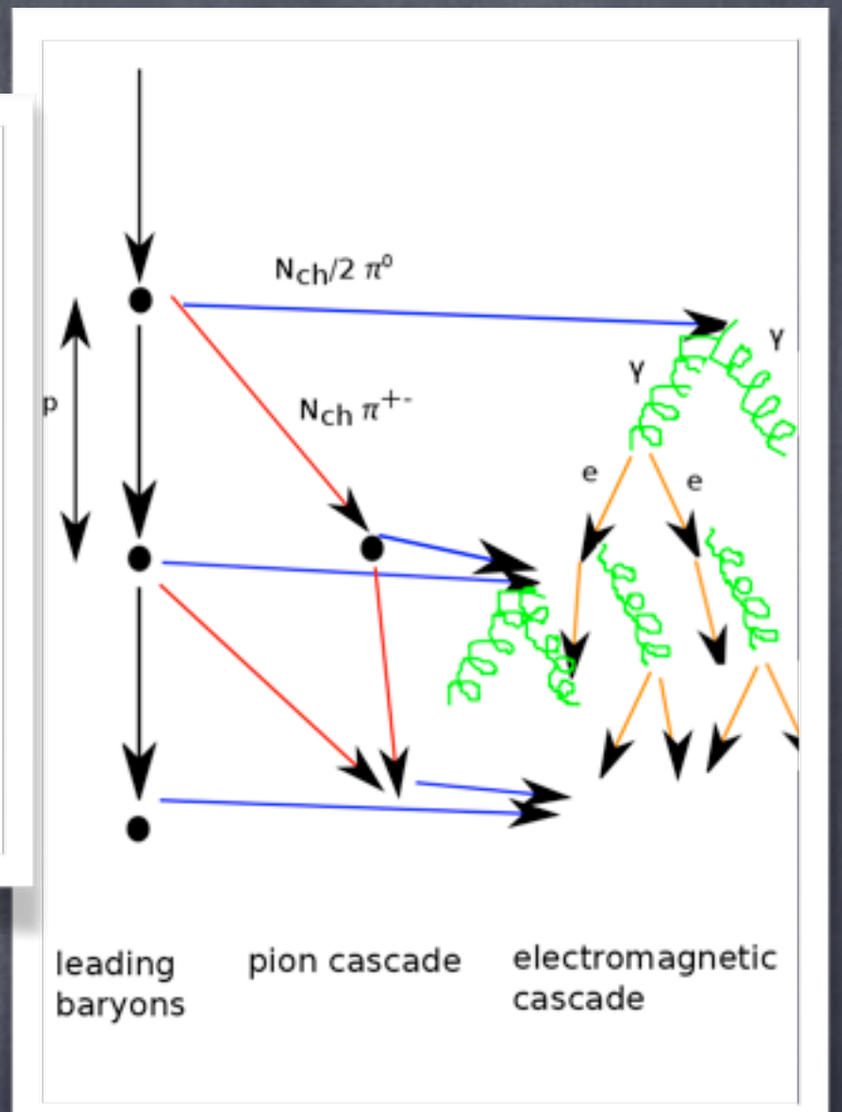

Pierre Auger Collaboration, PRL 117, 192001 (2016) [arXiv:1610.08509]

The muon number scales as

$$N_\mu \propto E_{\rm had} \propto (1 - f_{\pi^0})^N \ ,$$

with the fraction going into the electromagnetic channel $f_{\pi^0} \simeq \frac{1}{3}$ and the number of generations N strongly constrained by $X_{\rm max}$. Larger N_μ thus requires smaller f_{π^0} ! The production of ρ^0 could also play a role.

KASCADE data suggest a heavy composition below ~10^{18} eV possibly becoming lighter around 10^{18} eV

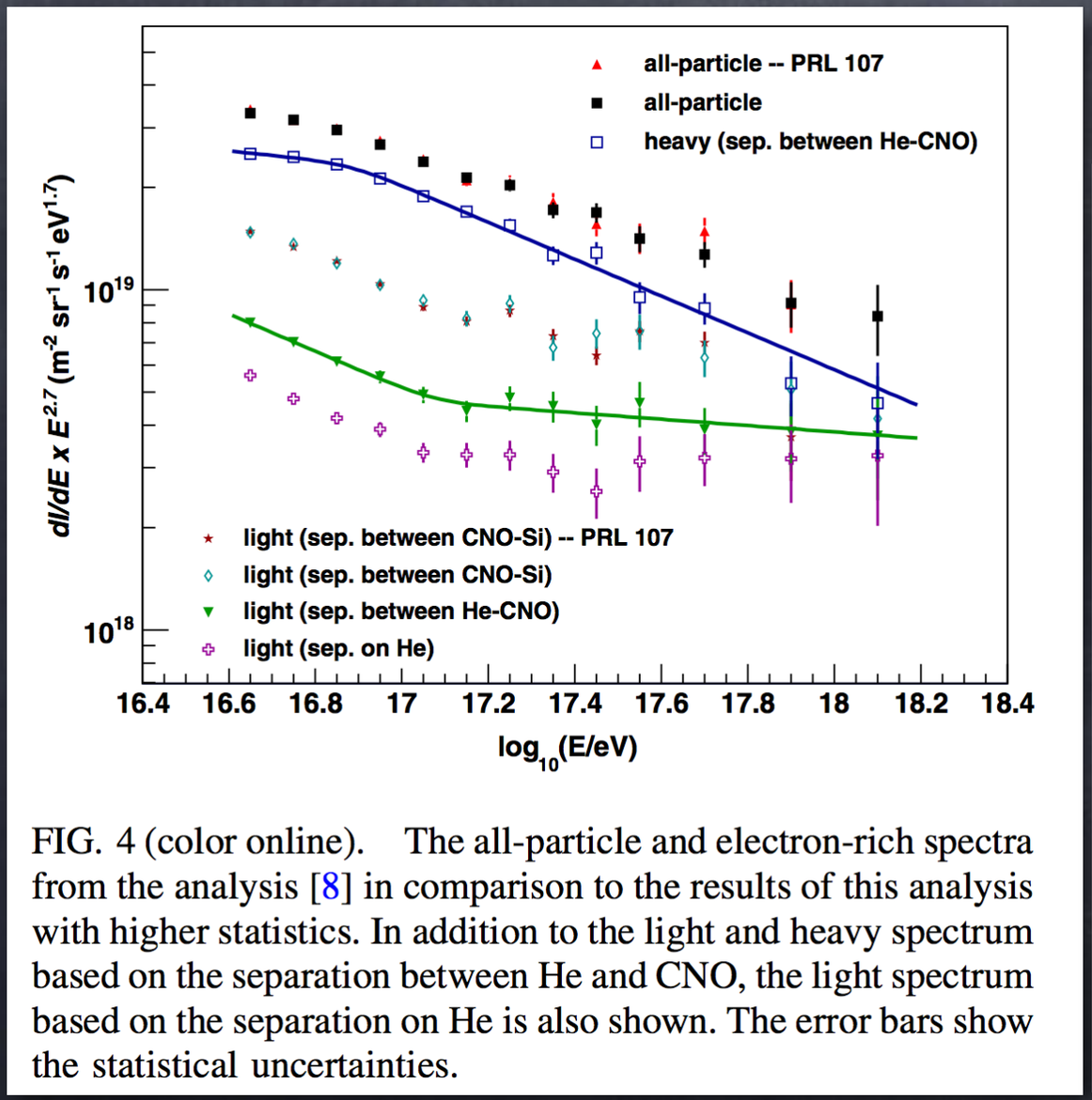

FIG. 4 (color online). The all-particle and electron-rich spectra from the analysis [8] in comparison to the results of this analysis with higher statistics. In addition to the light and heavy spectrum based on the separation between He and CNO, the light spectrum based on the separation on He is also shown. The error bars show the statistical uncertainties.

KASCADE Collaboration, Phys.Rev. D87 (2013) 081101,

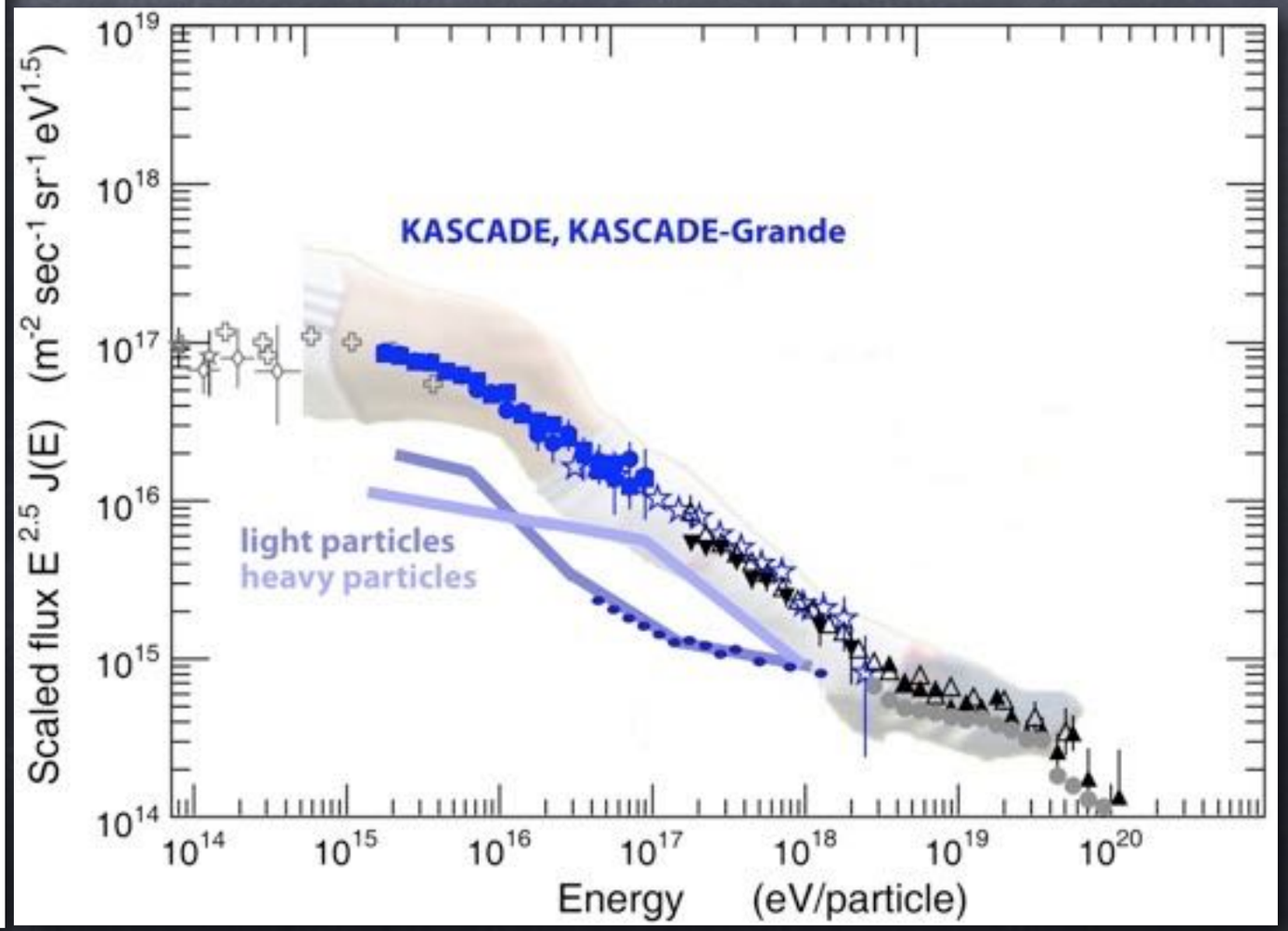

Latest Pierre Auger results suggest mixed composition around the Ankle

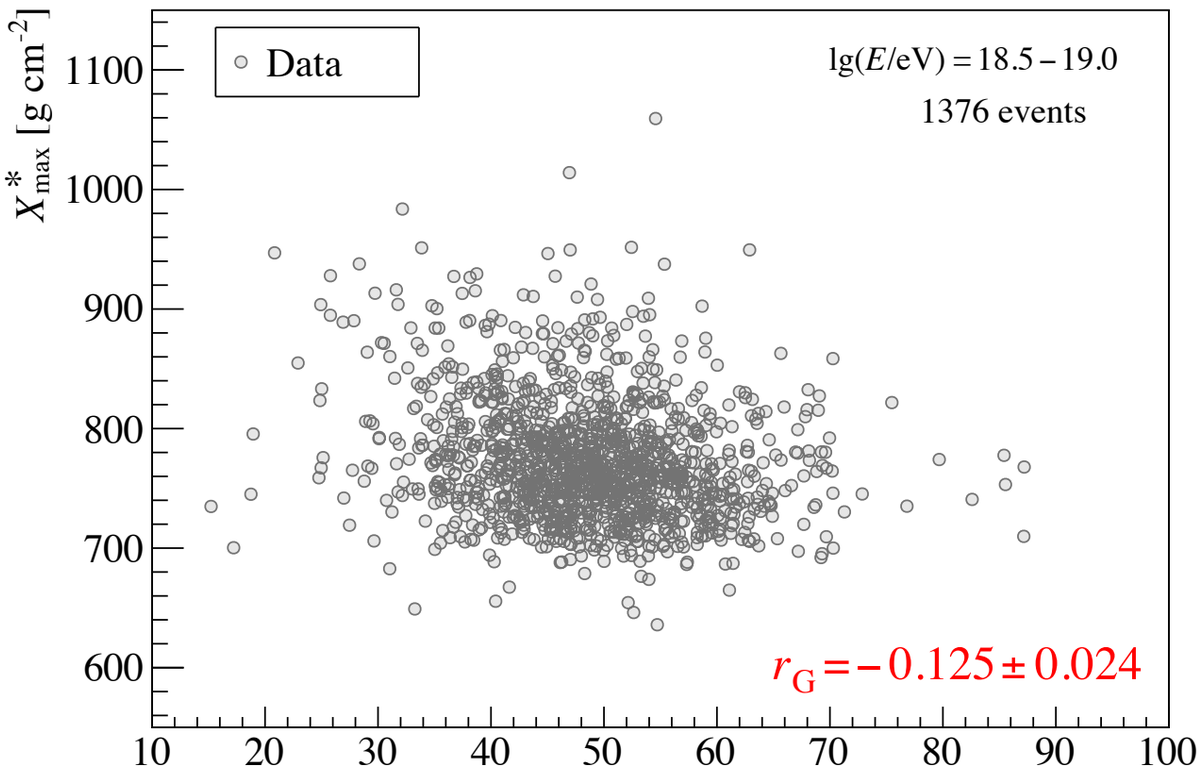

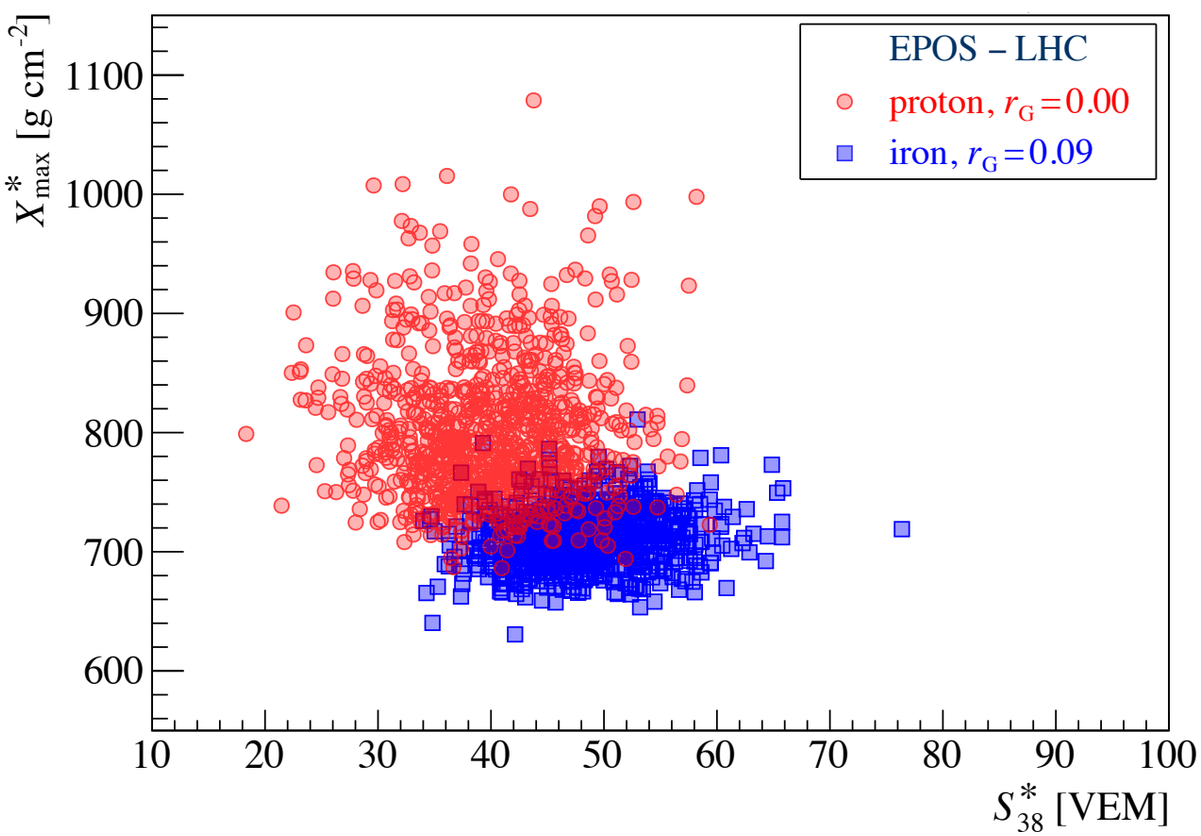

correlation between shower depth (measured by fluorescence detector) and particle density at 1km from shower core (measured by ground array) which is proxy for muon number is relatively insensitive to hadronic interaction models

Energy and zenith angle dependencies are projected out by scaling to 10 EeV and zenith angle 38 degrees.

Pure composition: zero or positive correlation mixed composition: negative correlation because large X_{max} correlates with light nuclei and small muon abundance

Pierre Auger collaboration, Phys. Lett. B 762, 288 (2016) [arXiv:1609.08567]

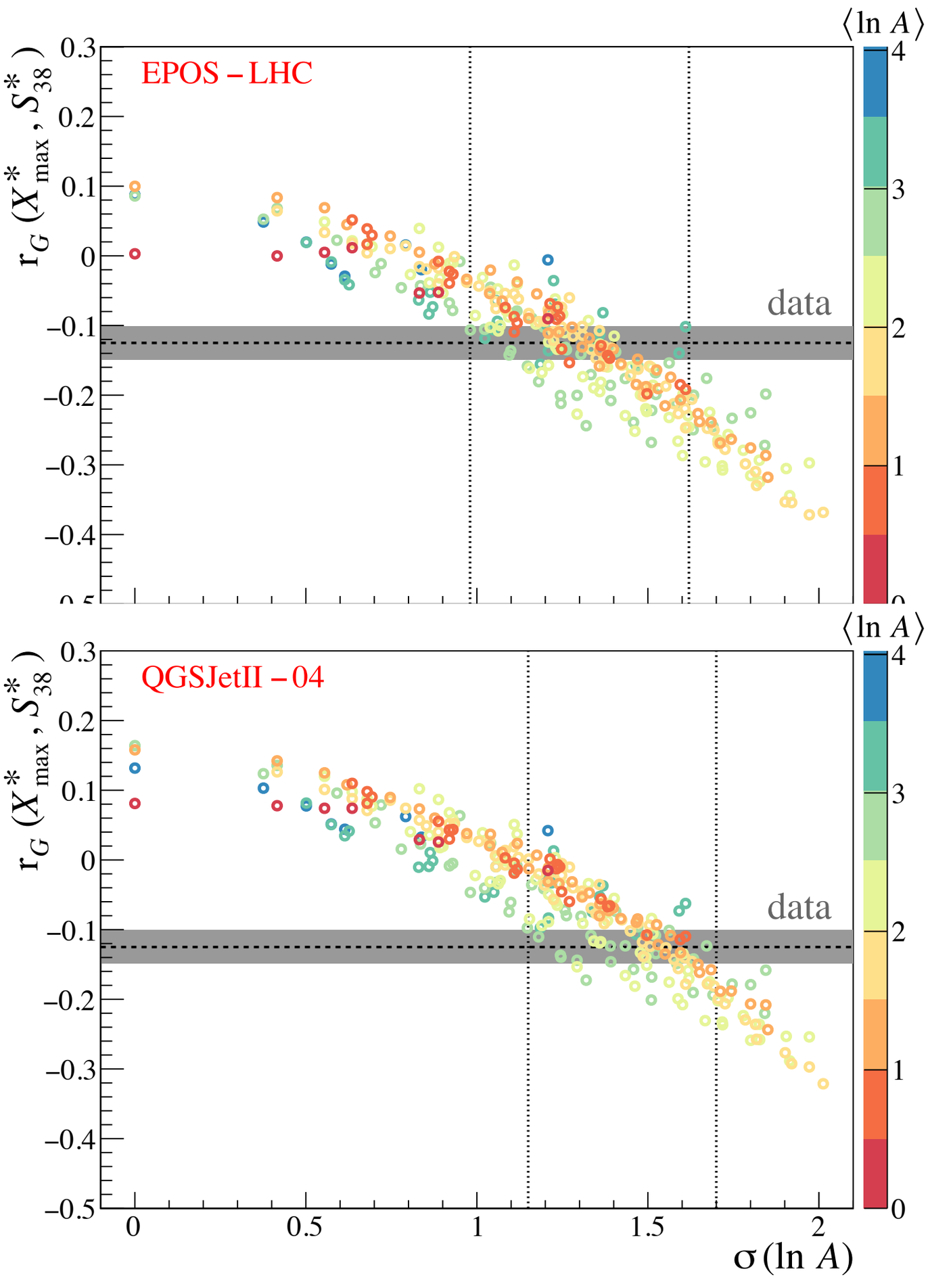

correlation coefficient versus measure of width of mass distribution:
larger spread of masses leads to smaller correlation coefficients

The observed correlations indicate a mixed composition including nuclei heavier than helium, $A > 4$ with mass spread $\sigma(\ln A)=1.35\pm0.35$

Summary of correlation coefficient: no significant energy trend

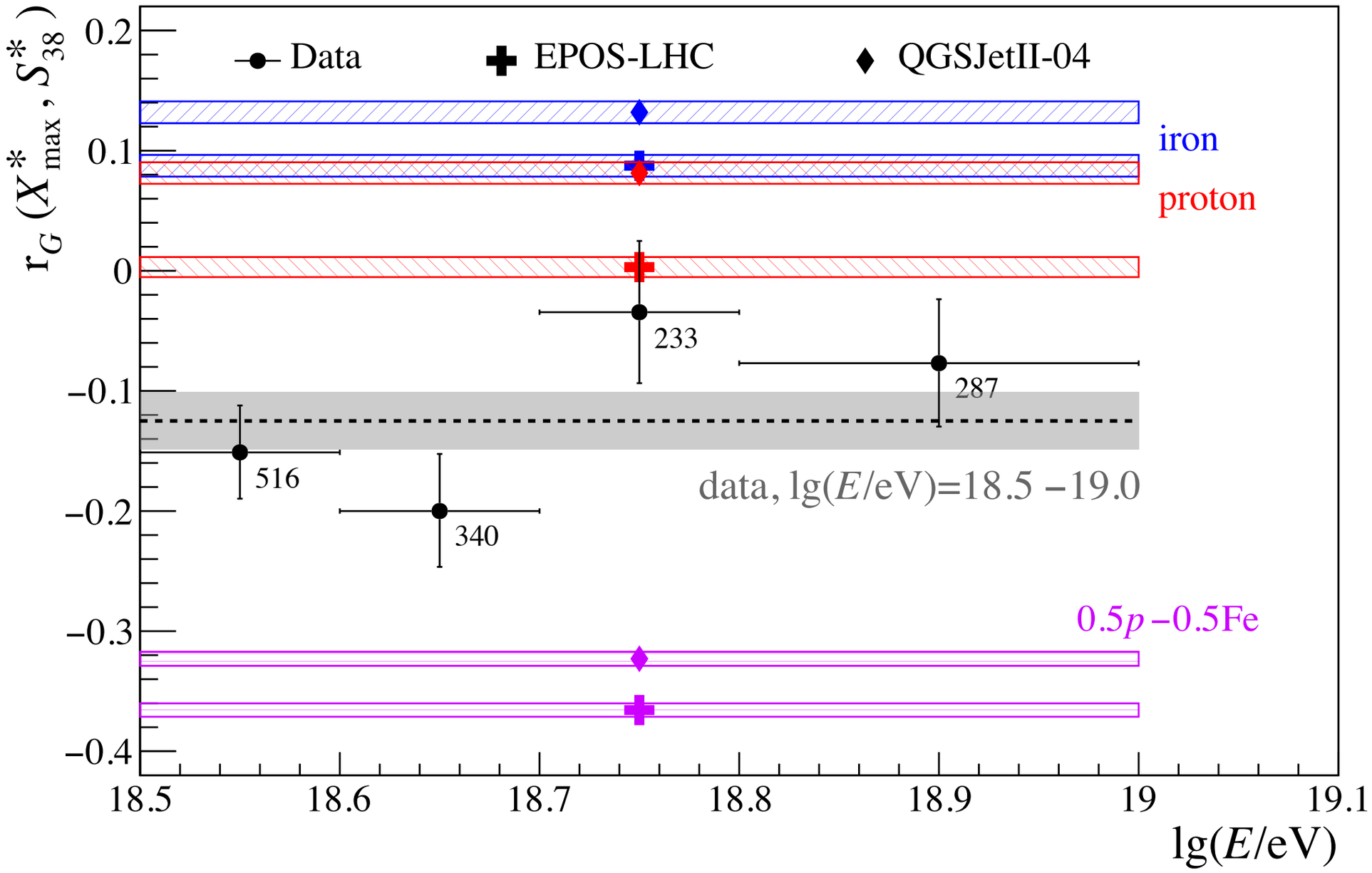

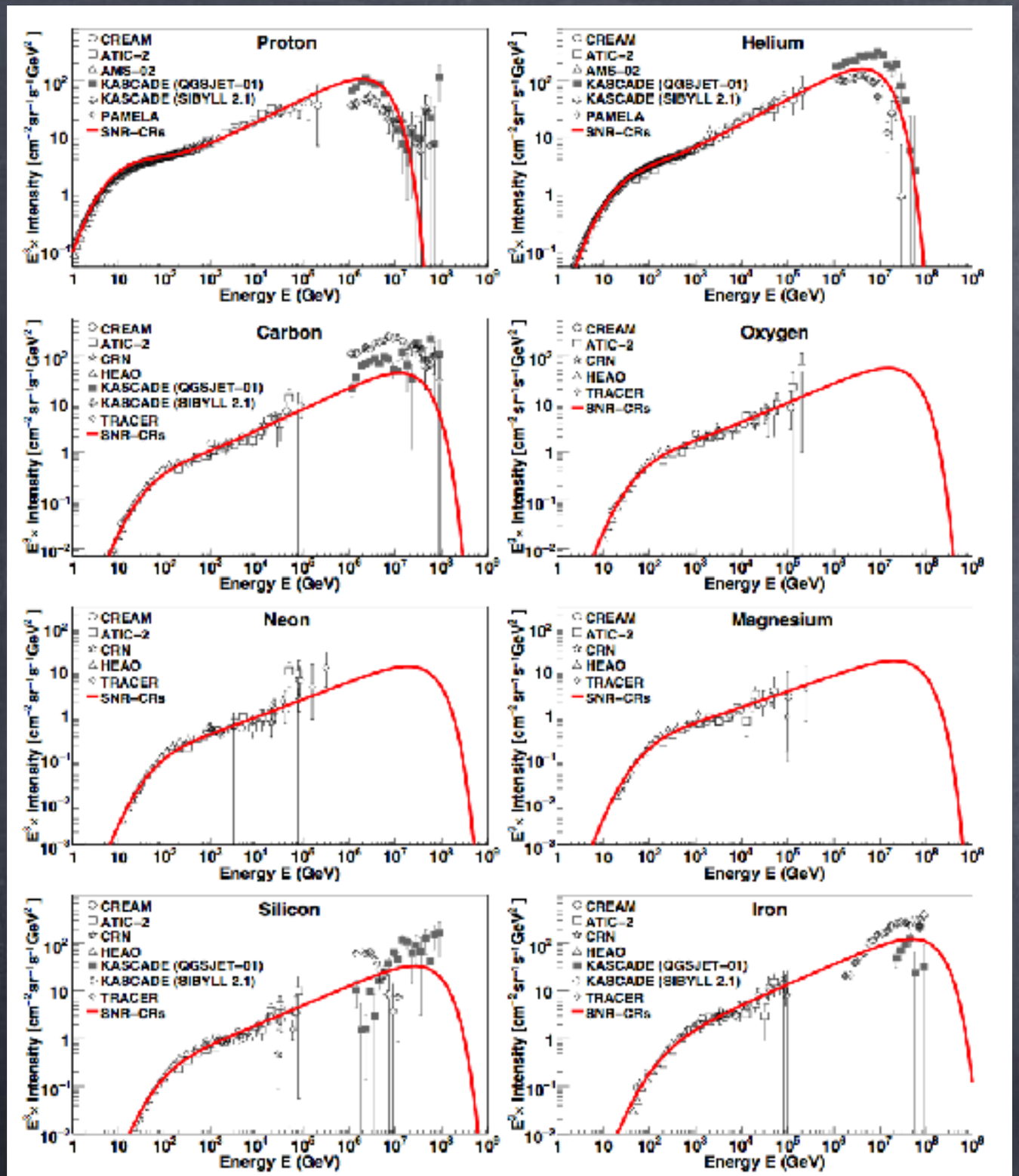

Fig. 1. Energy spectra for different cosmic ray elements. *Solid line*: Model prediction for the SNR CRs. *Data*: CREAM (Ahn et al. 2009; Yoon et al. 2011), ATIC 2 (Panov et al. 2007), AMS 02 (Aguilar et al. 2015a,b), PAMELA (Adriani et al. 2011), CRN (Müller et al. 1991; Swordy et al. 1990), HEAO (Engelmann et al. 1990), TRACER (Obermeier et al. 2011), and KASCADE (Antoni et al. 2005). Cosmic-ray source parameters (q, f) used in the calculation are given in Table 1. For the other model parameters (D_0, a, η, s), see text for details.

recent compilation of individual element spectra

S. Thoudam et al., arXiv:1605.03111

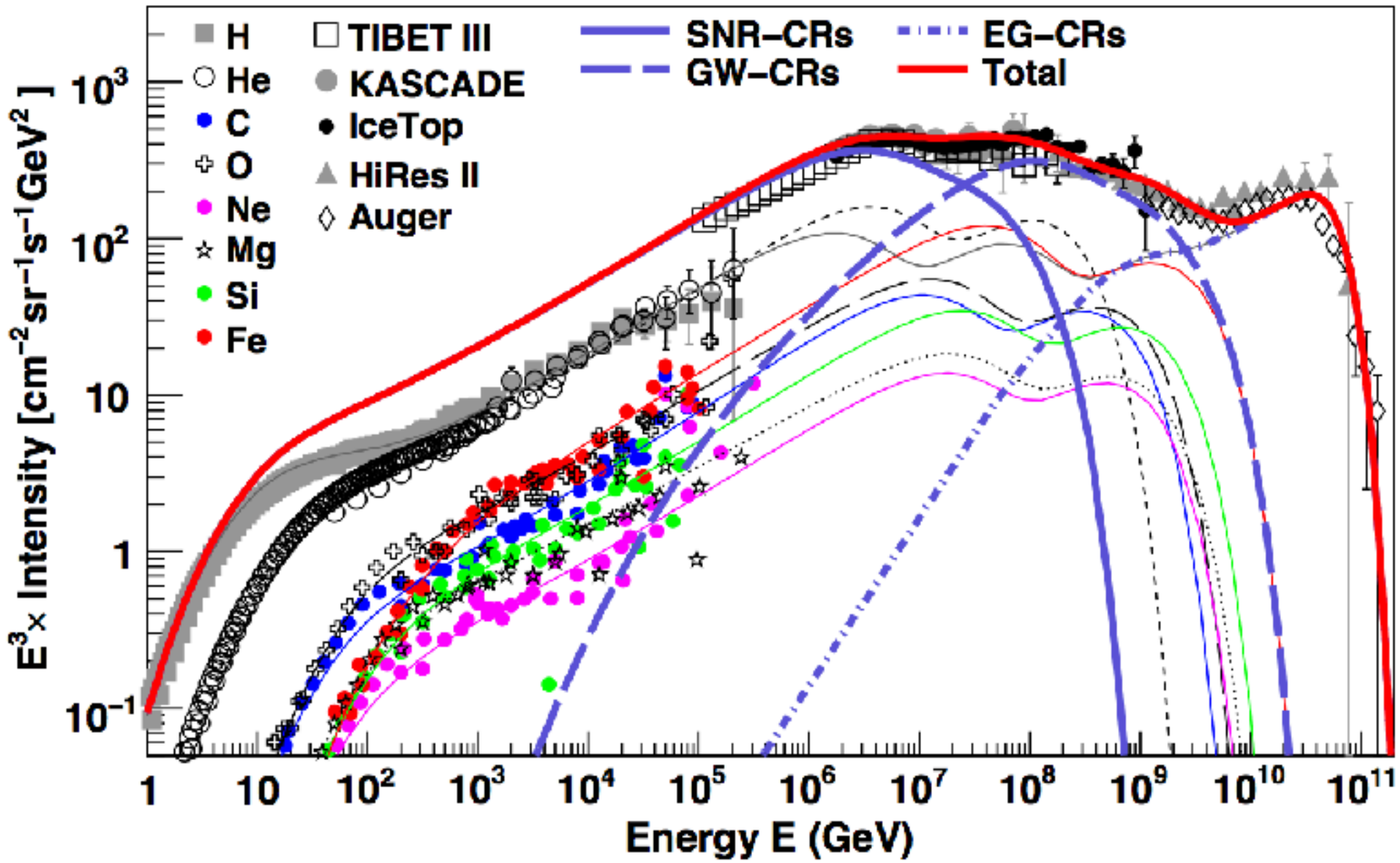

Fig. 5. Model prediction for the all-particle spectrum using the Galactic wind re-acceleration model. The thick solid blue line represents the total SNR-CRs, the thick dashed line represents GW-CRs, the thick dotted-dashed line represents EG-CRs, and the thick solid red line represents the total all-particle spectrum. The thin lines represent total spectra for the individual elements. For the SNR-CRs, an exponential energy cut-off for protons at $E_c = 3 \times 10^6$ GeV is assumed. See text for the other model parameters. Data are the same as in Figure 2.

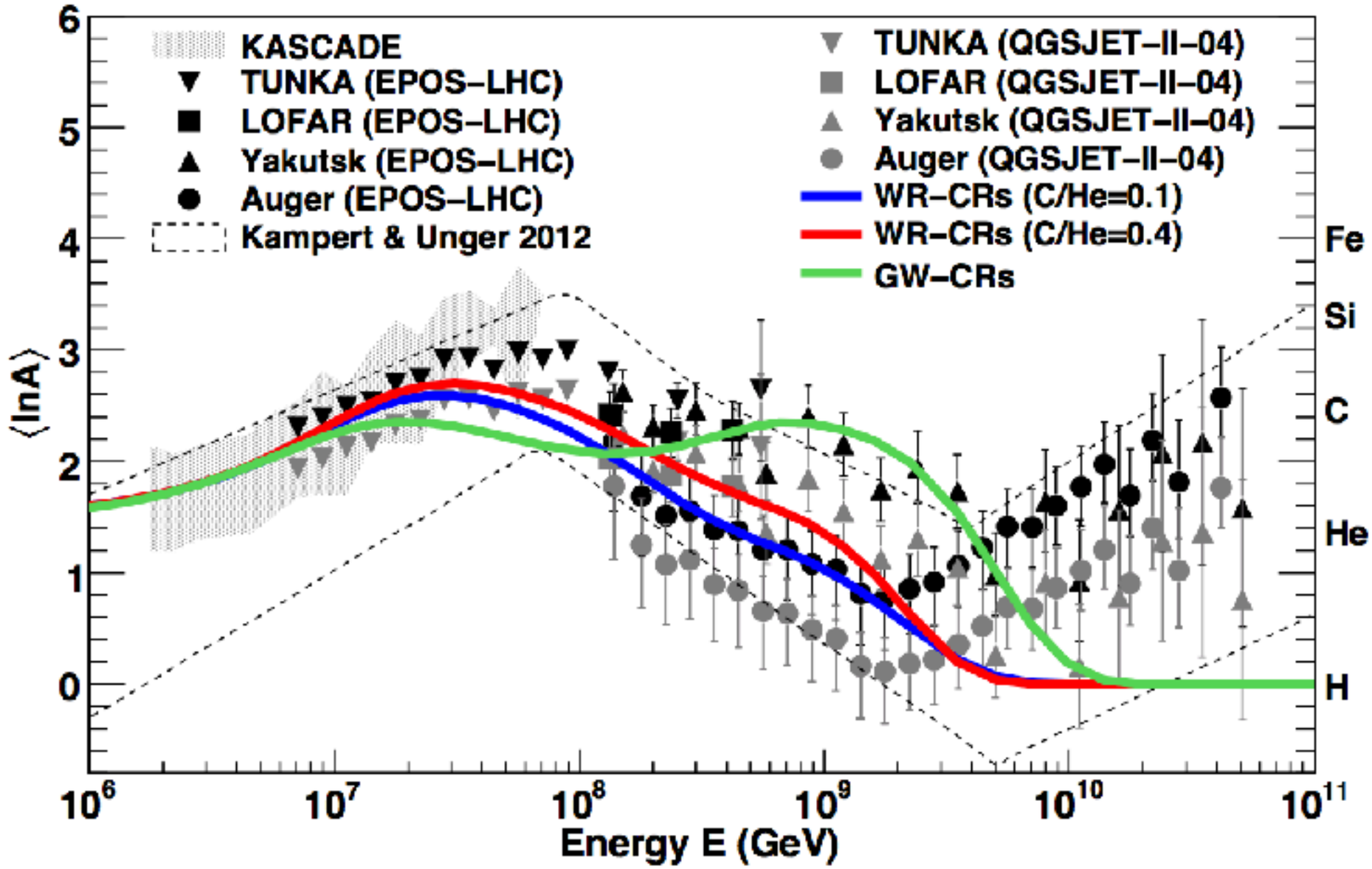

Fig. 8. Mean logarithmic mass, ⟨lnA⟩, of cosmic rays predicted using the three different models of the additional Galactic component: WR-CRs (C/He = 0.1), WR-CRs (C/He = 0.4), and GW-CRs. *Data*: KASCADE (Antoni et al. 2005), TUNKA (Berezhnev et al. 2013), LOFAR (Buitink et al. 2016), Yakutsk (Knurenko & Sabourov 2010), the Pierre Auger Observatory (Porcelli et al. 2015), and the different optical measurements compiled in Kampert & Unger (2012). The two sets of data points correspond to two different hadronic interaction models (EPOS-LHC and QGSJET-II-04) used to convert $X_{\max}$ values to ⟨lnA⟩.

Global Picture on Mass Composition

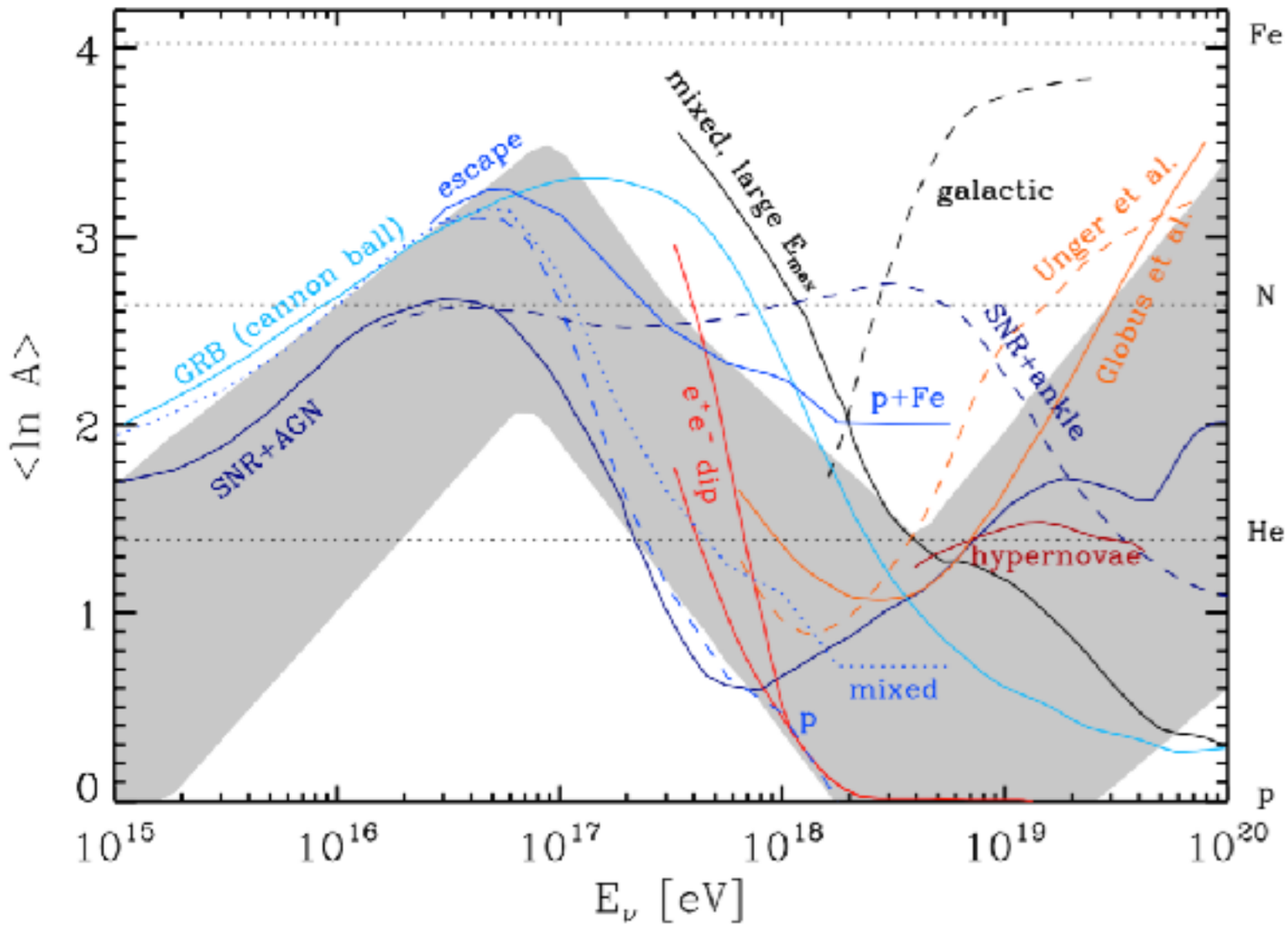

Fig. 5.8 The energy dependence of the average logarithmic mass predicetd by various models, as indicated and explained in more details in the text. The grey band represents the combined uncertainties resulting from systematic experimental errors and hadronic model uncertainties, based on data such as the ones shown in Fig. 5.7. The first minimum in $\langle \ln A \rangle$ at $\simeq 3 \times 10^{15}$ eV corresponds to the CR knee and the first maximum in $\langle \ln A \rangle$ at $\simeq 10^{17}$ eV corresponds to the *second knee*. Both the knee and the second knee could signify a rigidity dependent Peters cycle either due to the maximal rigidity reached at acceleration in supernova remnants or due to a transition to a propagation regime leading to faster CR leakage from the Galaxy. Finally, the second minimum in $\langle \ln A \rangle$ at $\simeq 5 \times 10^{18}$ eV signifies the *ankle*. Compare the CR spectrum shown in Fig. 5.6. Inspired by Ref. [231].

Indications of "Peters cycles" for galactic and extragalactic sources whose maximal energies are proportional to the charge Z and extend up to ~ 10^{17} and 10^{20} eV, respectively

G. Sigl, book to appear

see also K.-H.Kampert and M.Unger, Astropart.Phys. 35 (2012) 660

Composition and the Transition Galactic/Extragalactic Cosmic Rays

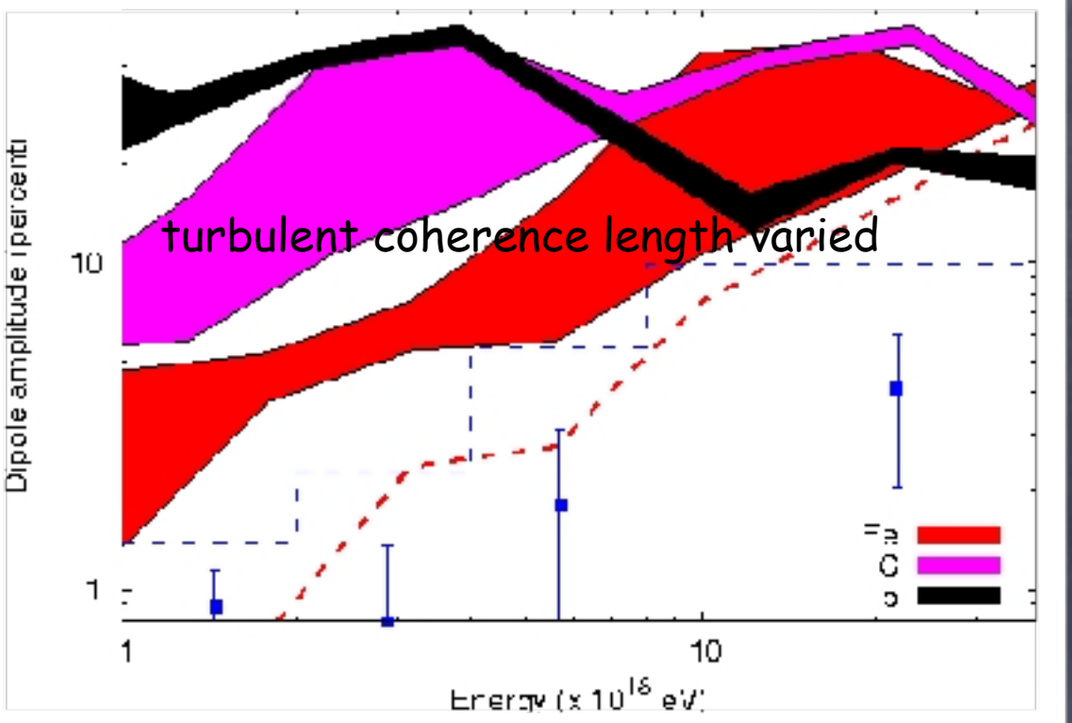

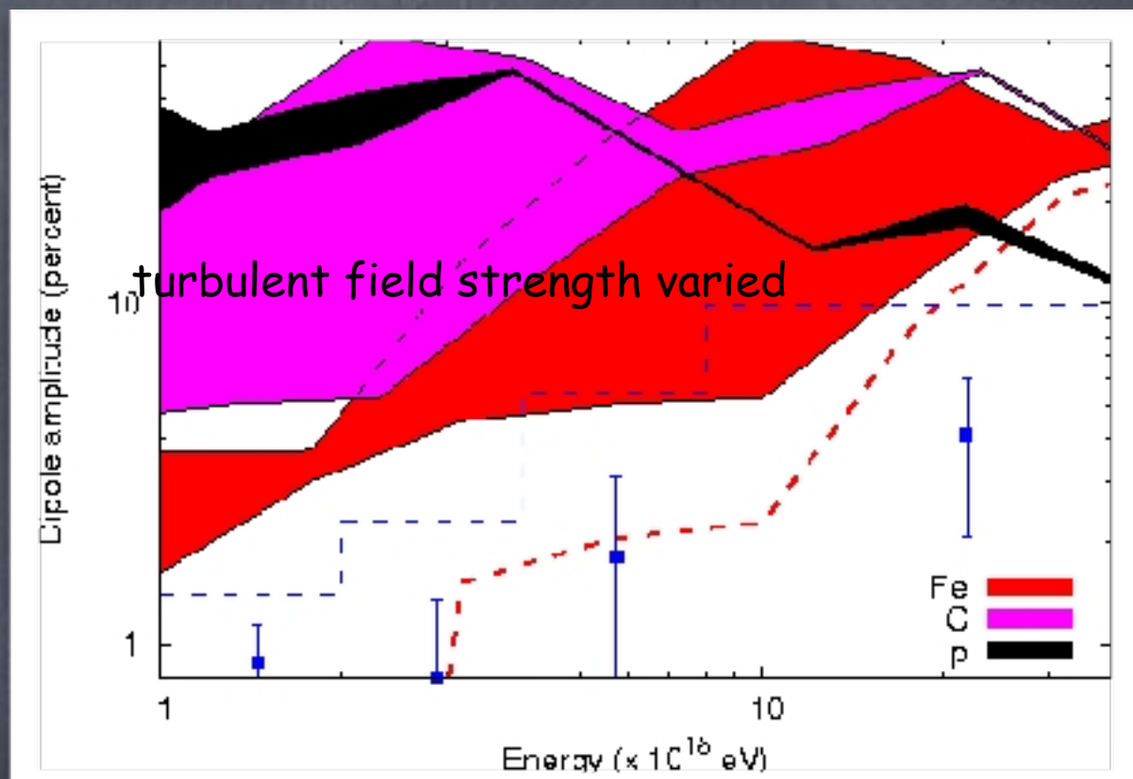

Giacinti, Kachelriess, Semikoz, Sigl,
JCAP 07 (2012) 031
and Pierre Auger Collaboration, Astrophys.J. 762 (2012) L13

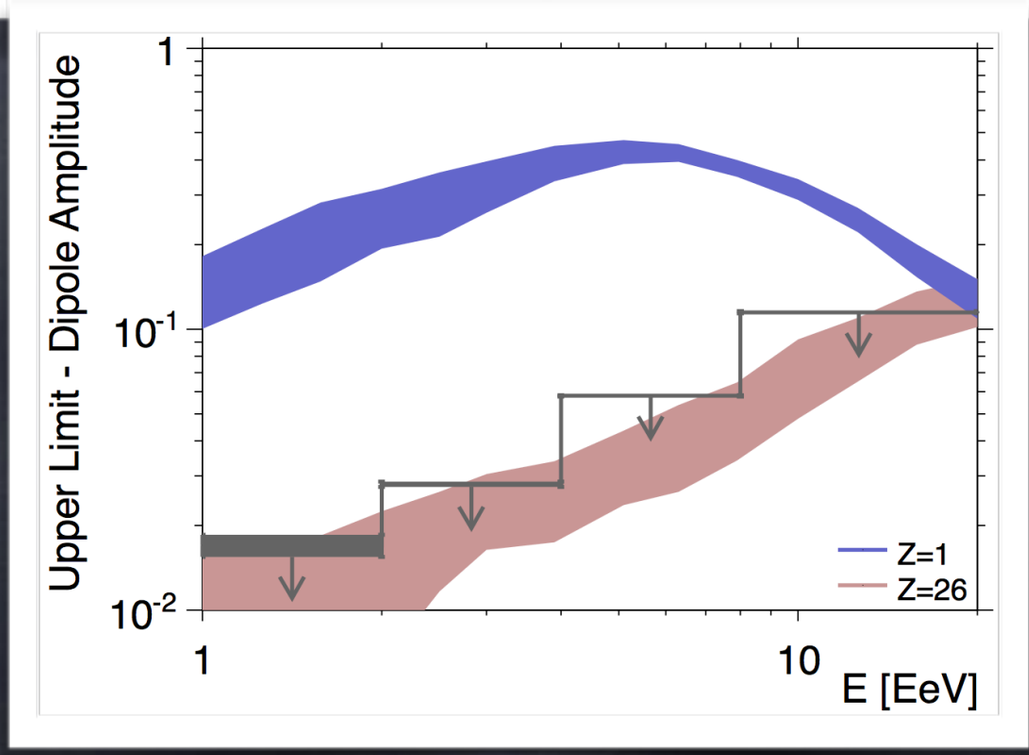

Light Galactic Nuclei produce too much anisotropy above ≃ 10^{18} eV. This implies:

1.) if composition around 10^{18} eV is light => probably extragalactic and ankle may be due to pair production by protons, but this scenario is now strongly disfavoured by Pierre Auger finding mixed composition at the ankle

2.) if composition around 10^{18} eV is heavy => transition could be at the ankle if Galactic nuclei are produced by sufficiently frequent transients, e.g. magnetars

QCD Predictions and Experimental Data

Cross sections depend on parton distribution functions and fragmentation functions which in turn depend on Q^2 and x. Dependence on former can be treated perturbatively, whereas the latter contains non-perturbative effects. The theoretical predictions depend on charm quark pole mass, factorisation and renormalisation scales, and the structure functions

Idea is to fit the non-perturbative components of these functions with as many measurements as possible to minimise uncertainties when extrapolating to energies and phase space inaccessible to direct experiments but relevant for cosmic ray physics.

Equivalent c.m. energy $\sqrt{s_{pp}}$ [TeV]

10^{-1} 1 10 10^{2}

0.9TeV 2.36TeV 7TeV 14TeV

LHC

Cross section (proton-air) [mb]

700 600 500 400 300 200

Nam et al. 1975 [30]
Siohan et al. 1978 [31]
Baltrusaitis et al. 1984 [2]
Mielke et al. 1994 [32]
Knurenko et al. 1999 [19]
Honda et al. 1999 [20]
Belov et al. 2007 [18]
Aglietta et al. 2009 [33]
Aielli et al. 2009 [34]
This work

QGSJet01c
QGSJetII.3
Sibyll 2.1
Epos 1.99

10^{11} 10^{12} 10^{13} 10^{14} 10^{15} 10^{16} 10^{17} 10^{18} 10^{19} 10^{20}

Energy [eV]

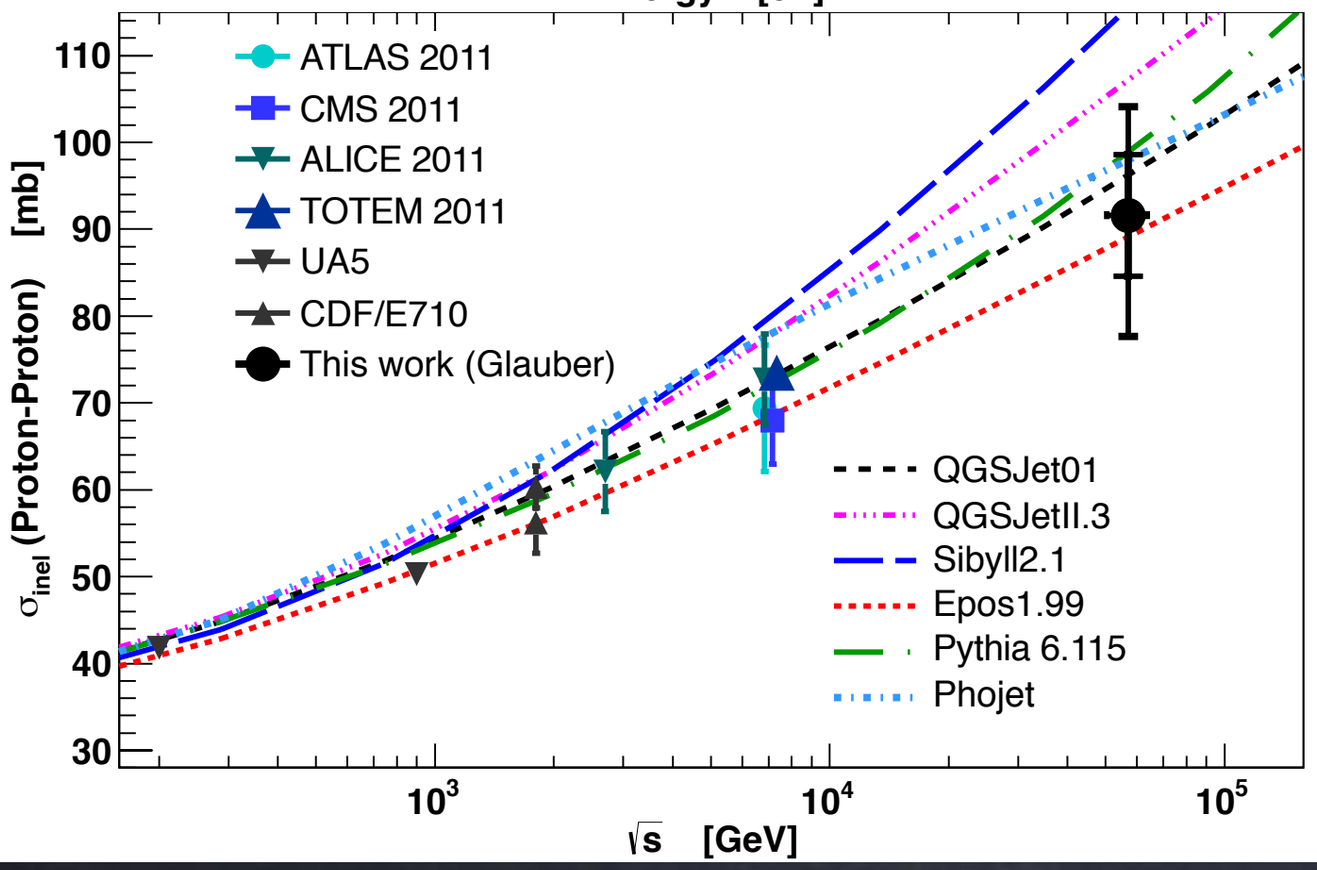

Example: Total proton-proton and proton-air cross sections:

p-air cross section derived from exponential tail of depth of shower maxima

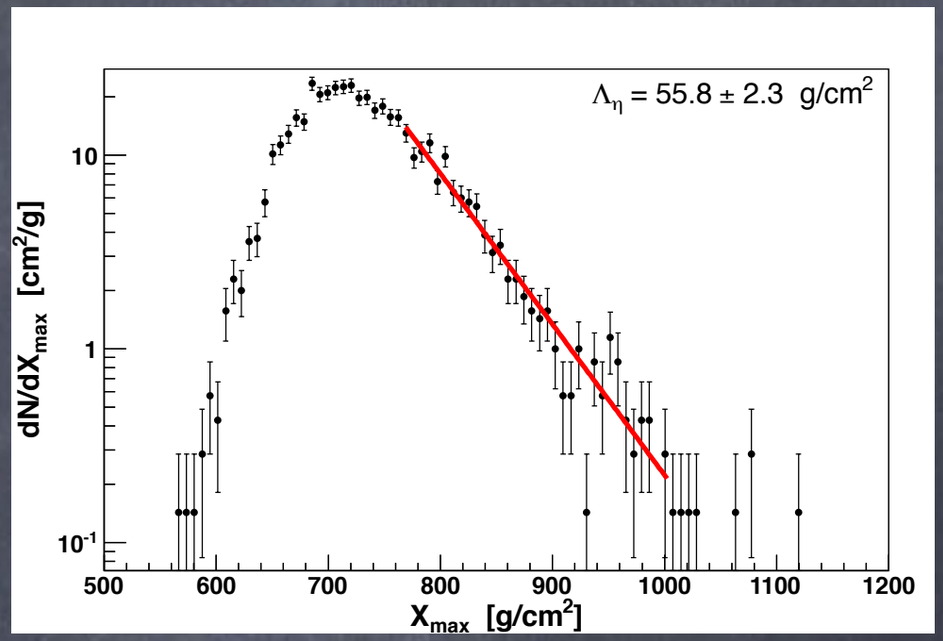

pp cross section derived from Glauber model

Pierre Auger Collaboration, PRL 109, 062002 (2012)

comparison of parton distribution functions

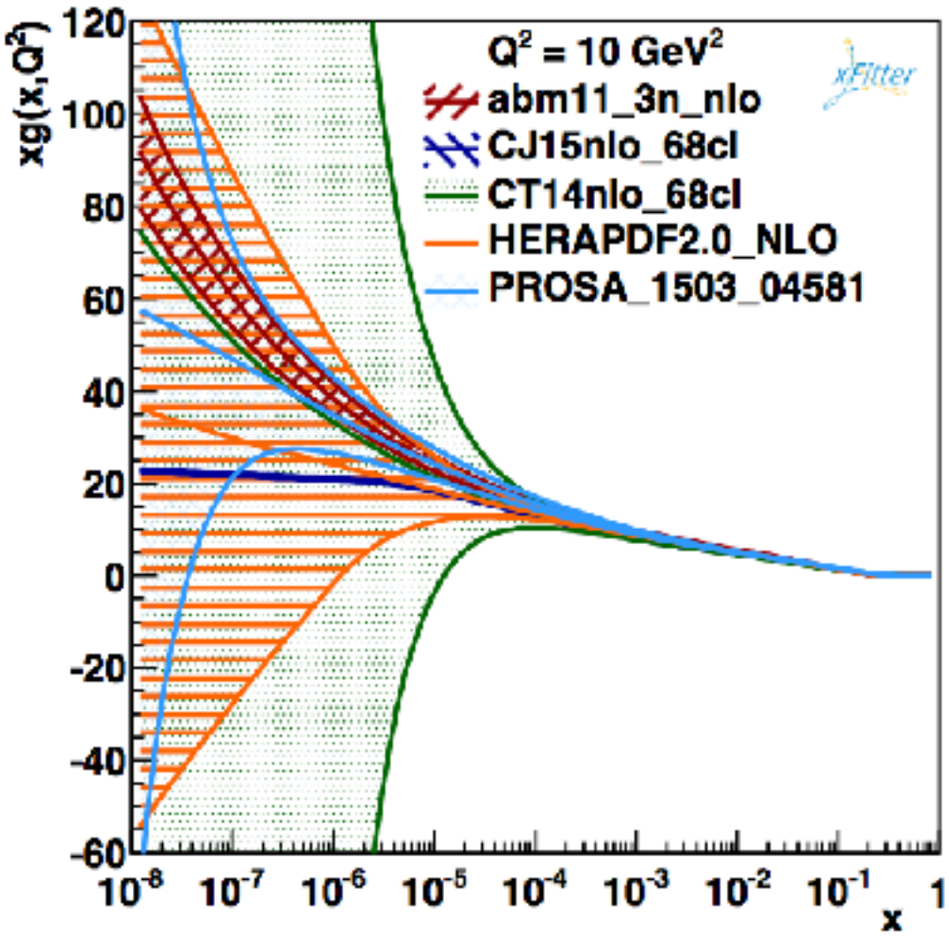

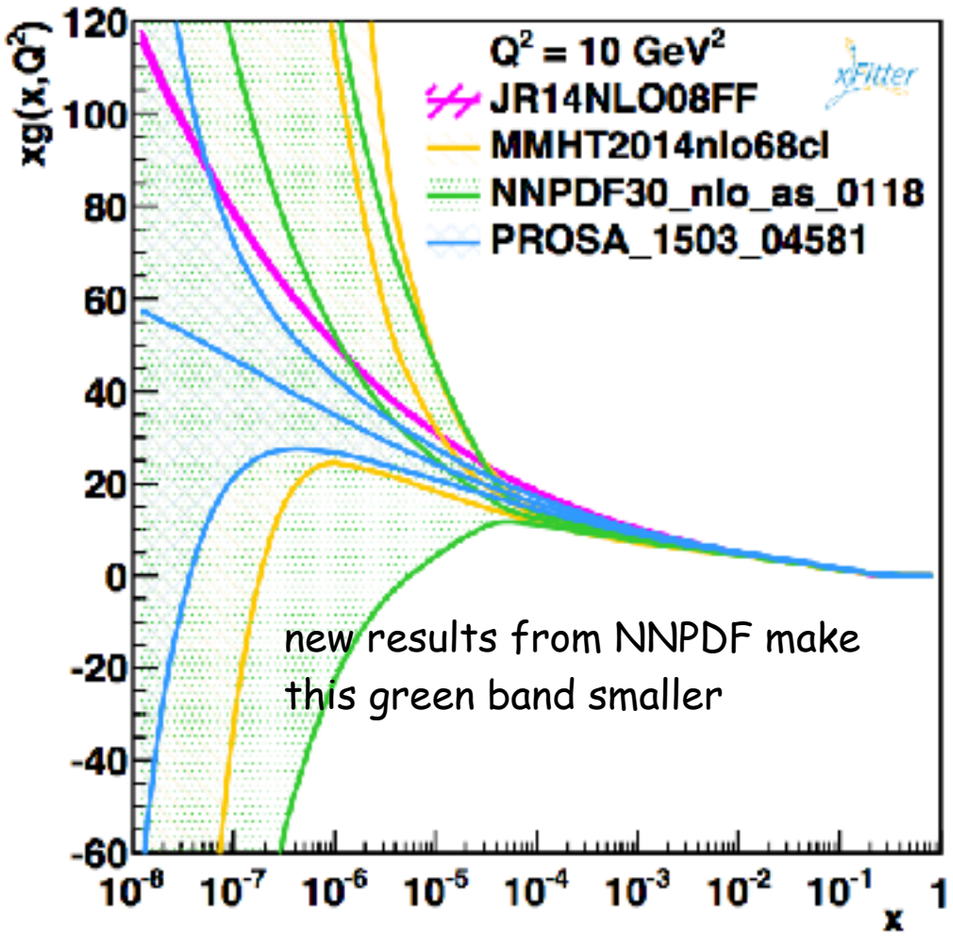

Figure 4. The PROSA gluon distribution compared to ABM11 [48], CJ15 [49], CT14 [50], HERAPDF2.0 [52] (left) and JR14 [51], MMHT2014 [53] and NNPDF3.0 [54] (right) at NLO at the scale of 10 GeV^2. The plots are obtained using the `Xfitter` program [56, 57]. Note that the ABM11, PROSA and JR14 PDFs employ the fixed flavour number scheme (with $n_f = 3$) in the fit of DIS data, whereas CT14, CJ15, HERAPDF2.0, NNPDF and MMHT use different implementations of the variable flavour number scheme, so the latter distributions should only be compared qualitatively to the former ones.

M. Garzelli et al., arXiv:1611.03815

pp-> D^{+-}+X @ sqrt(s) = 7 TeV,

ABM11 PDF, data: LHCb collaboration, Nucl.Phys B871, 1 (2013)

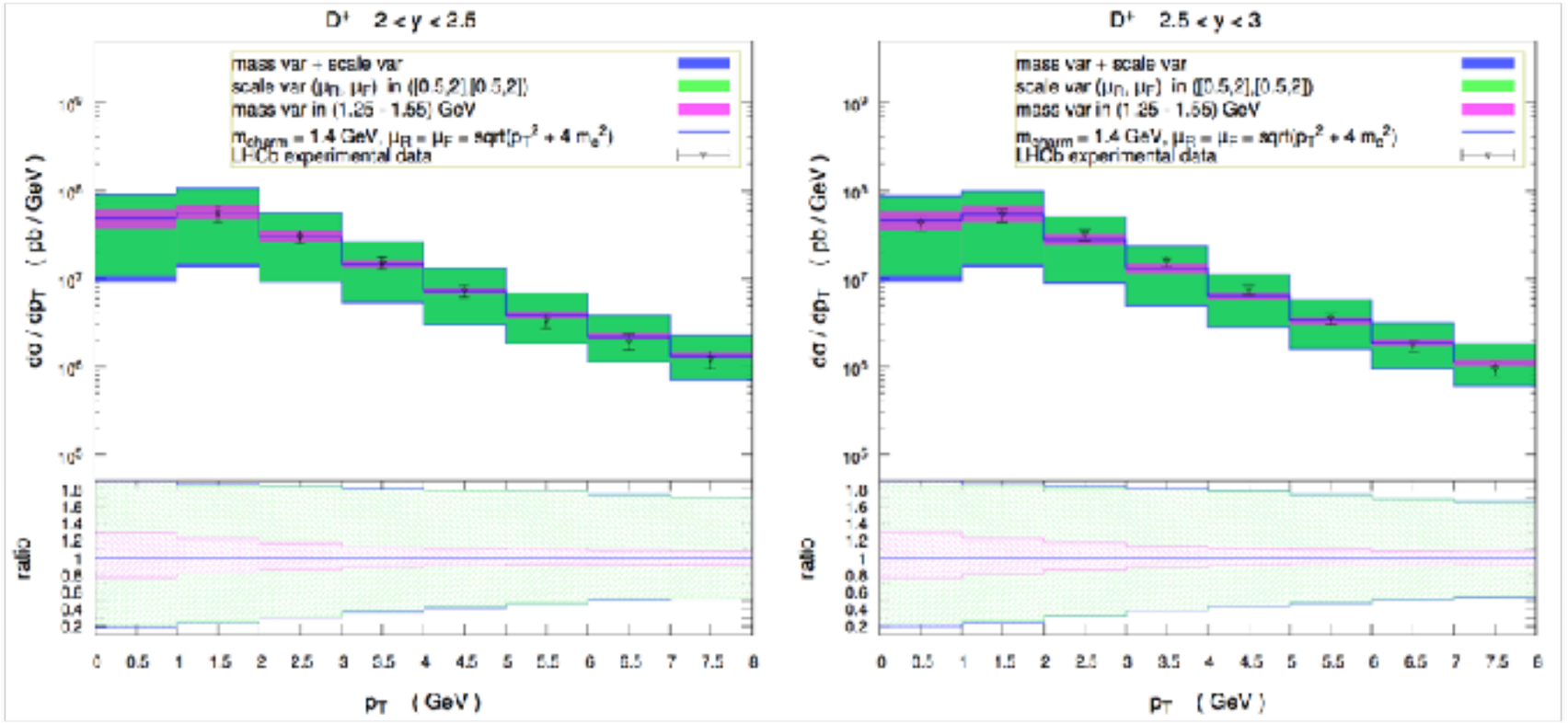

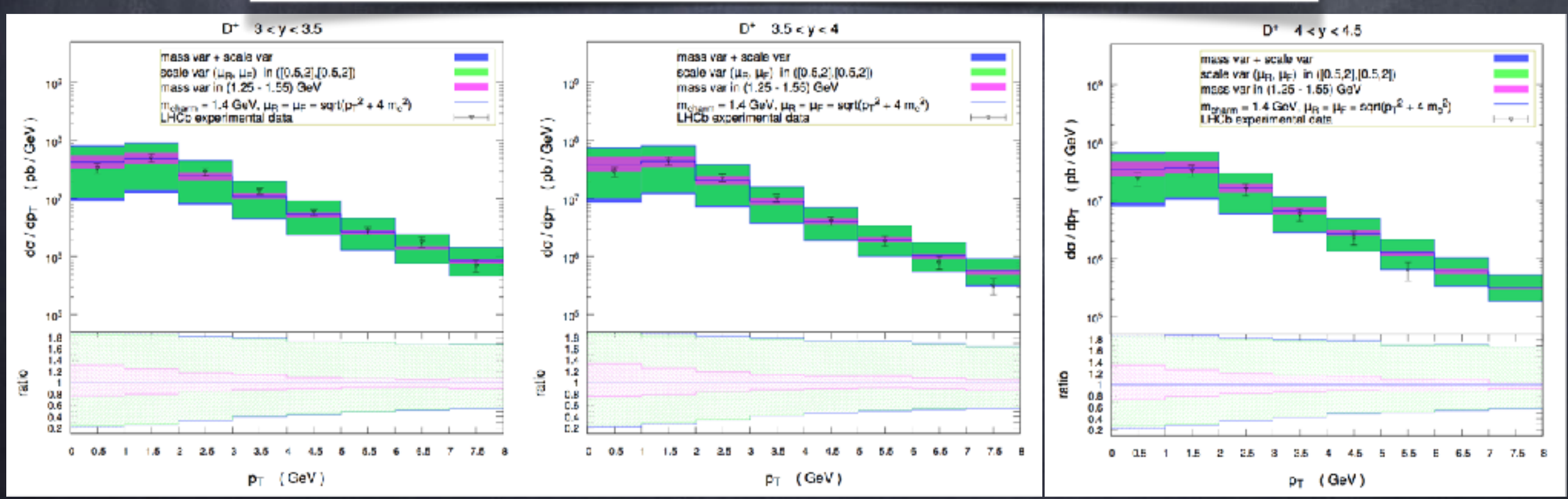

M. Benzke et al., PoS LL2016, 060 (2016)

pp-> D^{+-}+X @ sqrt(s) = 13 TeV,

ABM11 PDF, data: LHCb collaboration, JHEP 1603, 159, 1609, 013 (2016)

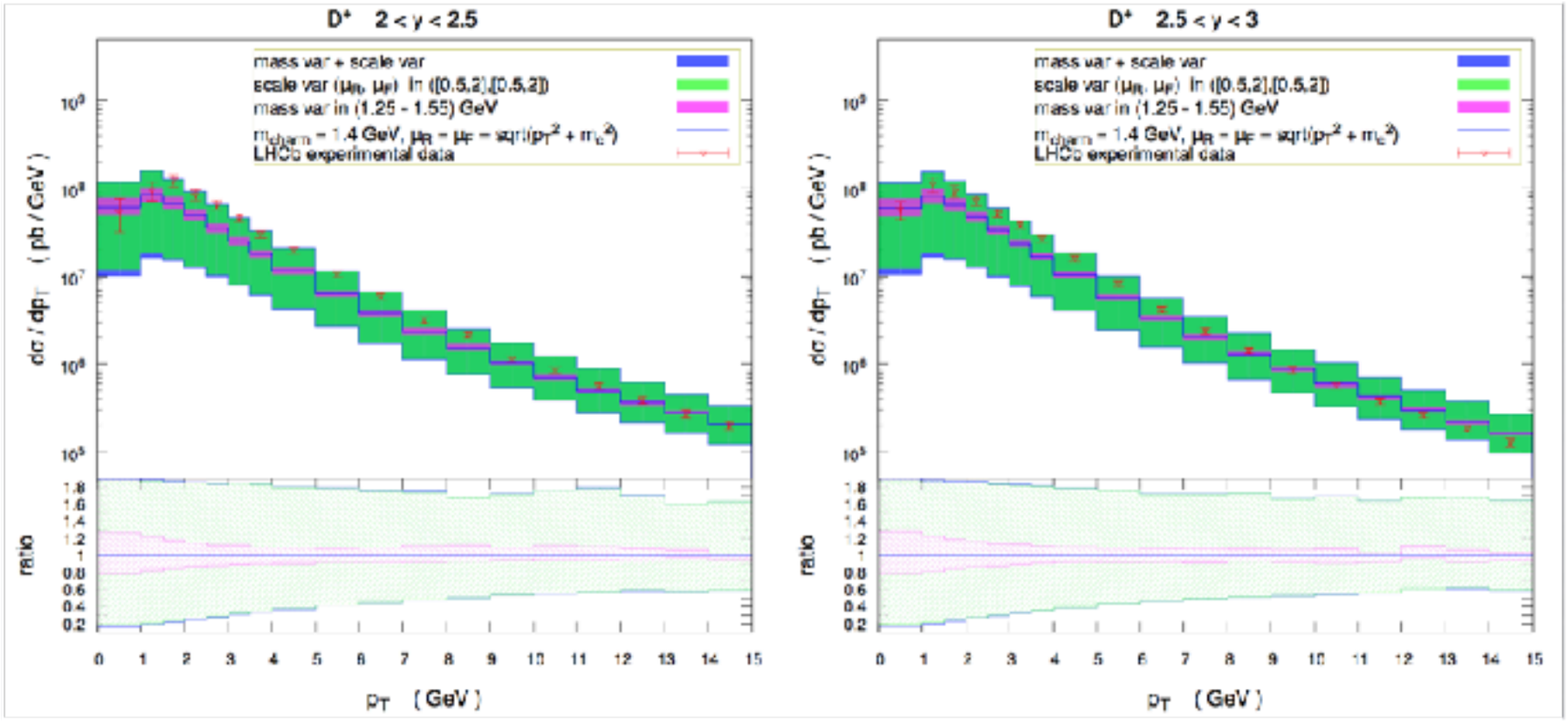

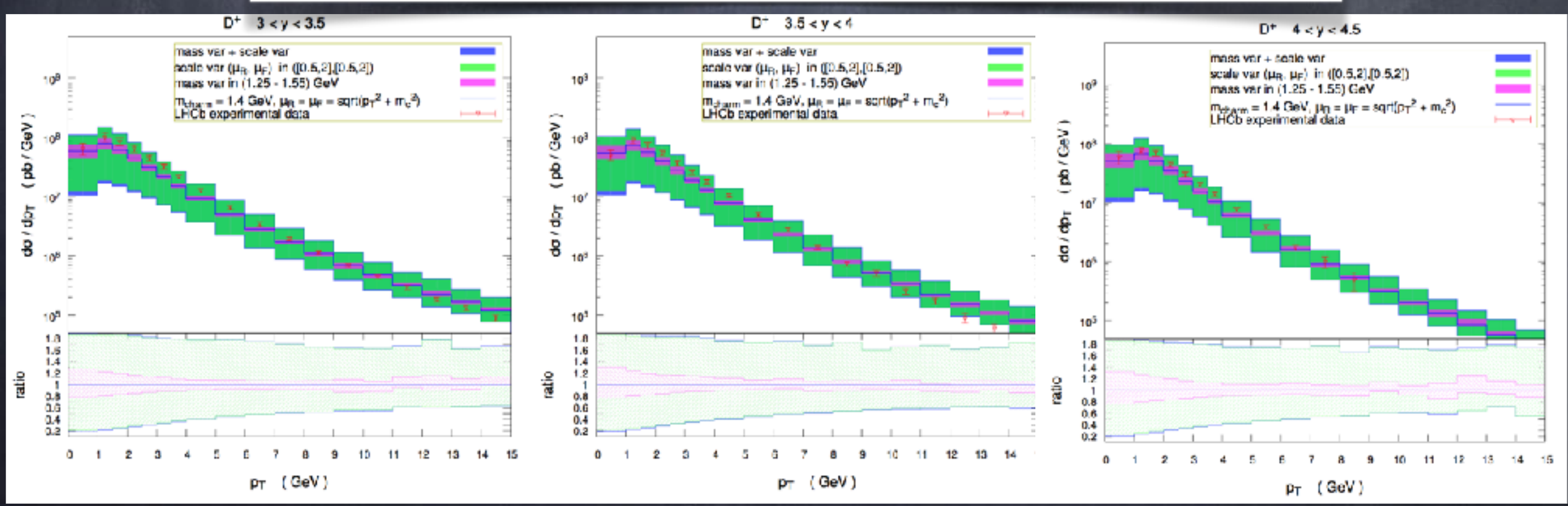

M. Benzke et al., PoS LL2016, 060 (2016)

pp-> D^{+-}+X @ sqrt(s) = 13 TeV,
PROSA PDF,data: LHCb collaboration, JHEP 1603, 159, 1609, 013 (2016)

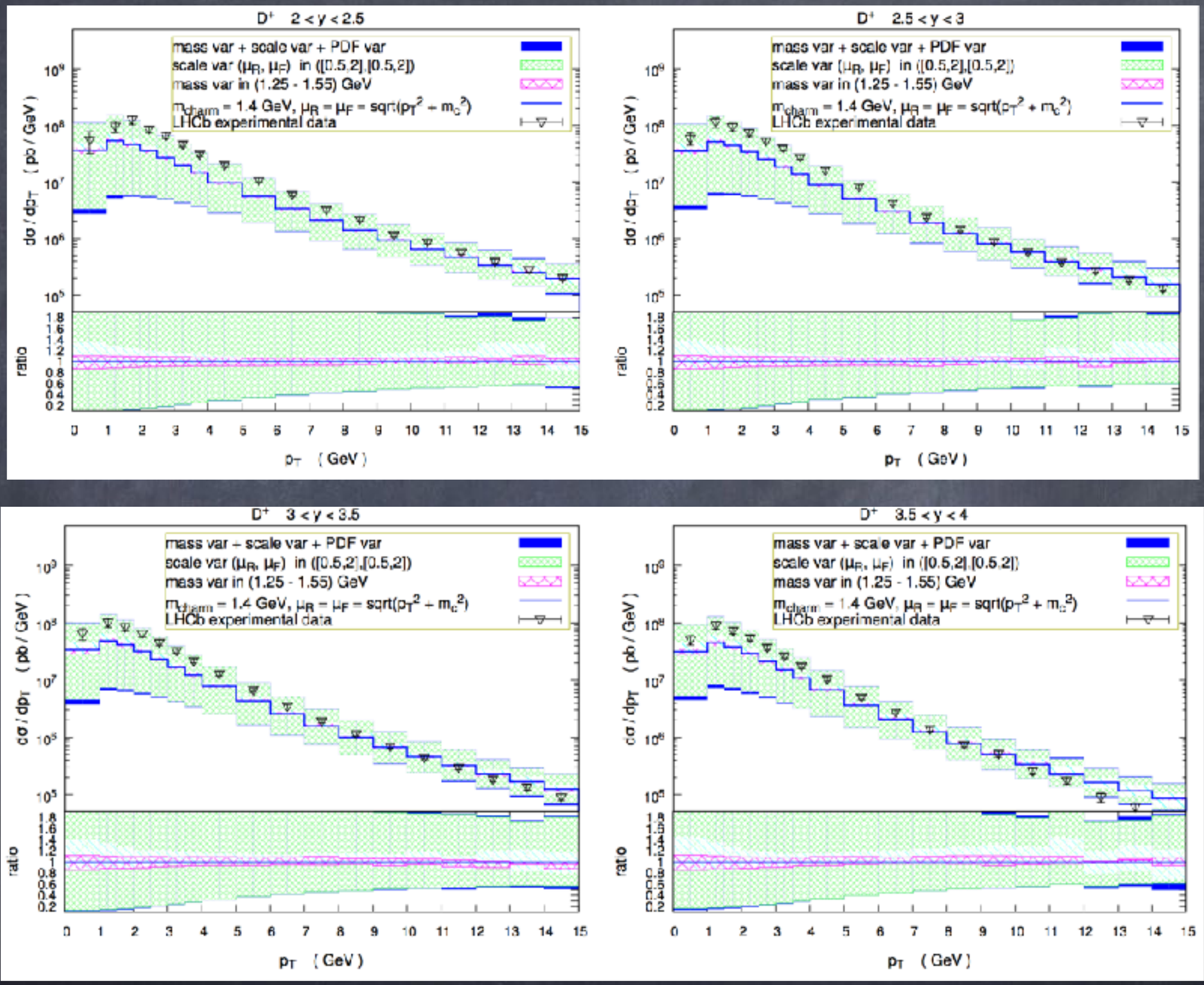

M. Garzelli et al., arXiv:1611.03815

Comments

theoretical uncertainties larger than experimental uncertainties; this can be reduced, however, by taking ratios of suitable quantities (e.g. at different energies or at different rapidities at same energy), as have been presented by LHCb

parton distribution functions used in literature:
ABM, CT14, JR14, CJ15, HERAPDF, MMHT, …
specifically with LHCb: PROSA and NNPDF3.0: partly large uncertainties at low x

theoretical cross sections known to NLO for $d\sigma/dp_T$ (not yet NNLO) and to NNLO for total cross section σ

inclusive charm pair production

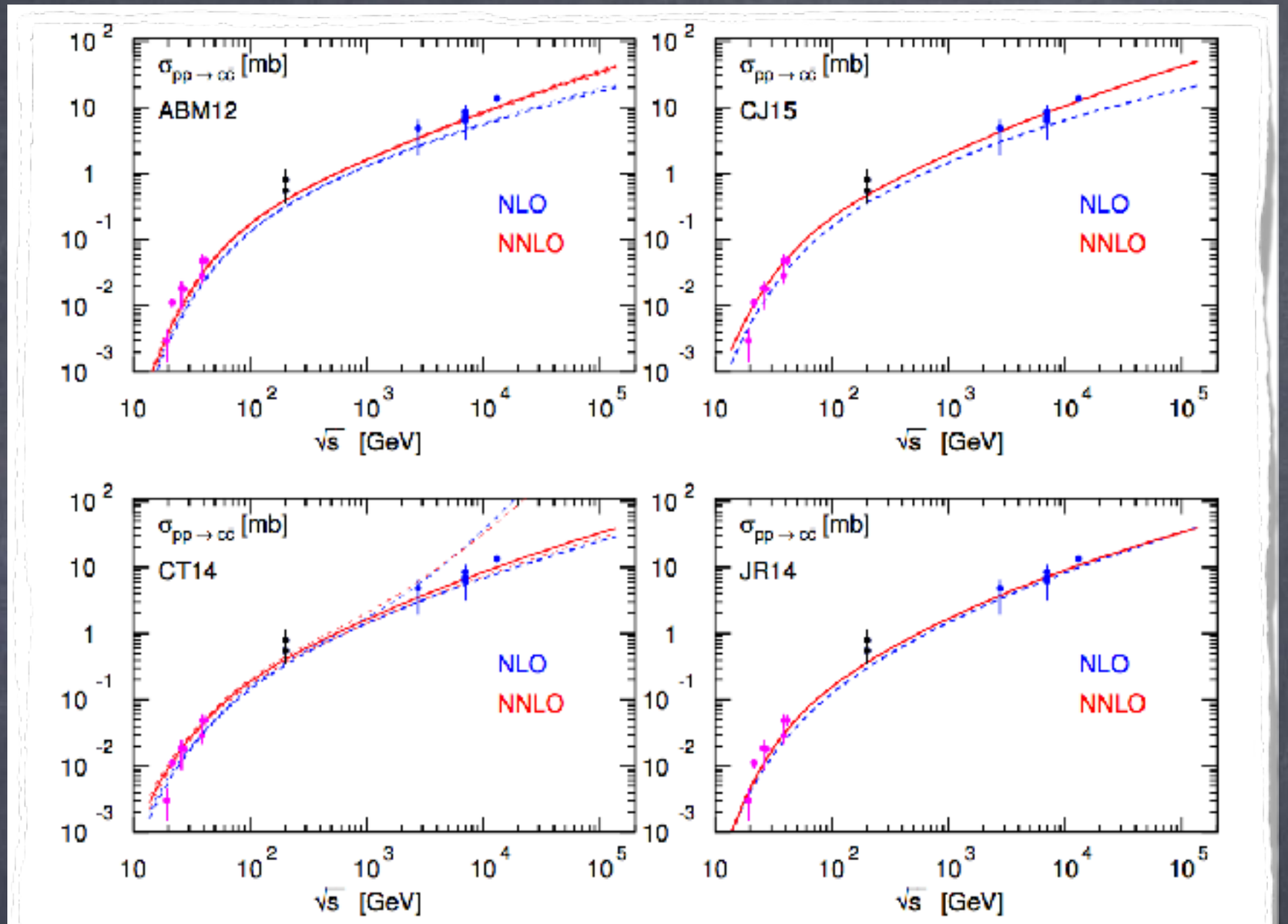

FIG. 16: Theoretical predictions for the total $pp \to c\bar{c}$ cross section as a function of the center-of-mass energy $\sqrt{s}$ at NLO (dashed lines) and NNLO (solid lines) QCD accuracy in the $\overline{\rm MS}$ mass scheme with $m_c(m_c) = 1.27$ GeV and scale choice $\mu_R = \mu_F = 2m_c(m_c)$ using the central PDF sets (solid lines) of ABM12 [2], CJ15 [1], CT14 [3] and JR14 [5] and the respective PDF uncertainties (dashed lines). The predictions for ABM12 (CJ15) use the NNLO (NLO) PDFs independent of the order of perturbation theory. See text for details and references on the experimental data from fixed target experiments and colliders (STAR, PHENIX, ALICE, ATLAS, LHCb).

A. Accardi et al., Eur.Phys.J. C76, 471 (2016) [arXiv:1603.08906]

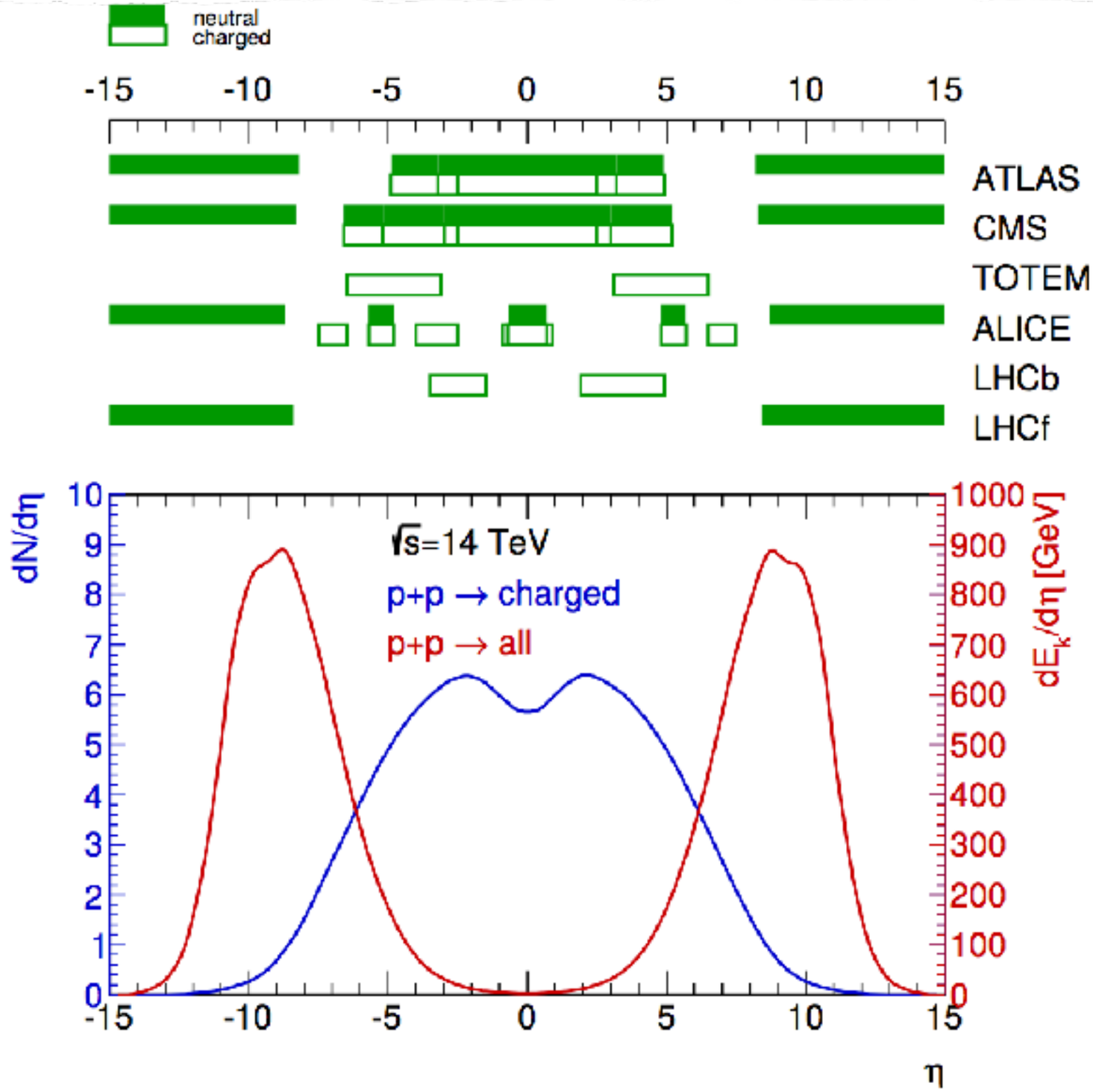

Figure 2.4: Energy and particle flow as a function of pseudorapidity at the LHC. The green bands represent the coverage of different detector components. Plot by R. Ulrich.

Felix Riehn, PhD thesis

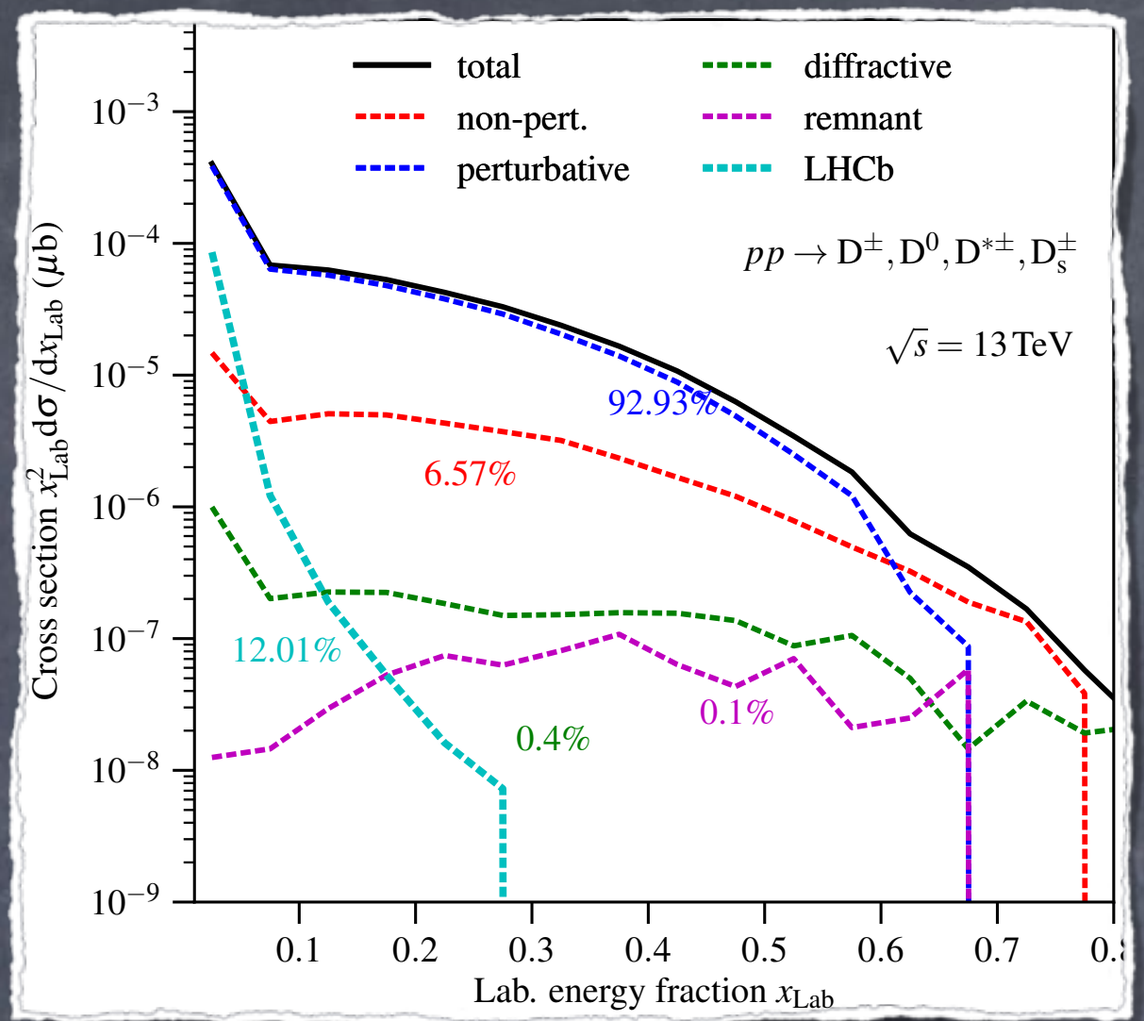

LHCb phase space contribution to charmed meson production in pp

no large non-perturbative contributions seem to be necessary when comparing with the data

at low energy measured charm production cross sections seem larger than N*LO QCD predictions for the ABM PDFs

Calculation of Atmospheric Lepton Fluxes

$$\frac{d\phi_j}{dX} = -\frac{\phi_j}{\lambda_{j,int}} - \frac{\phi_j}{\lambda_{j,dec}} + \sum_{k\neq j} S_{\rm prod}(k \to j) + \sum_{k\neq j} S_{\rm decay}(k \to j) + S_{\rm reg}(j \to j)\,.$$

These are known as cascade equations. There is a critical energy above which interactions dominate over decay; for charged pions it is about 20 GeV,
for charmed mesons it is much higher, ~ 10^7 GeV

$$S_{\rm prod}(k \to j) = \int_{E_j}^{\infty} dE_k \frac{\phi_k(E_k, X)}{\lambda_k(E_k)} \frac{1}{\sigma_k} \frac{d\sigma_{k\to j}(E_k, E_j)}{dE_j} \sim \frac{\phi_k(E_j, X)}{\lambda_k(E_j)} Z_{kj}(E_j)\,,$$

$$S_{\rm decay}(j \to l) = \int_{E_l}^{\infty} dE_j \frac{\phi_j(E_j, X)}{\lambda_j(E_j)} \frac{1}{\Gamma_j} \frac{d\Gamma_{j\to l}(E_j, E_l)}{dE_l} \sim \frac{\phi_j(E_l, X)}{\lambda_j(E_l)} Z_{jl}(E_l)\,.$$

Most relevant for us is the all-nucleon flux which depends both on the all-particle flux and the mass composition

Flux models used in Garzelli et al., JHEP10 (2015) 115

Cosmic Ray primary all-nucleon flux

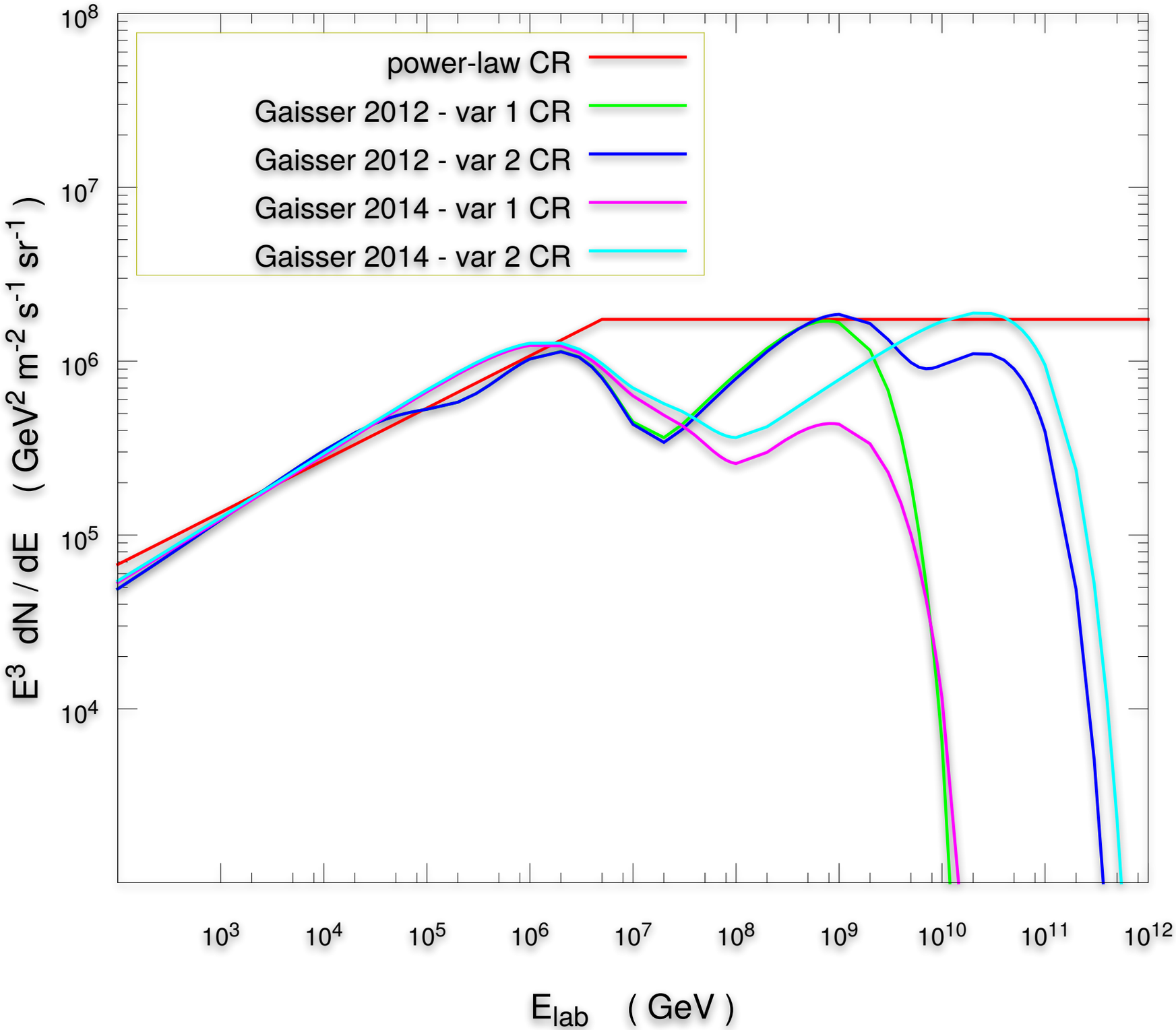

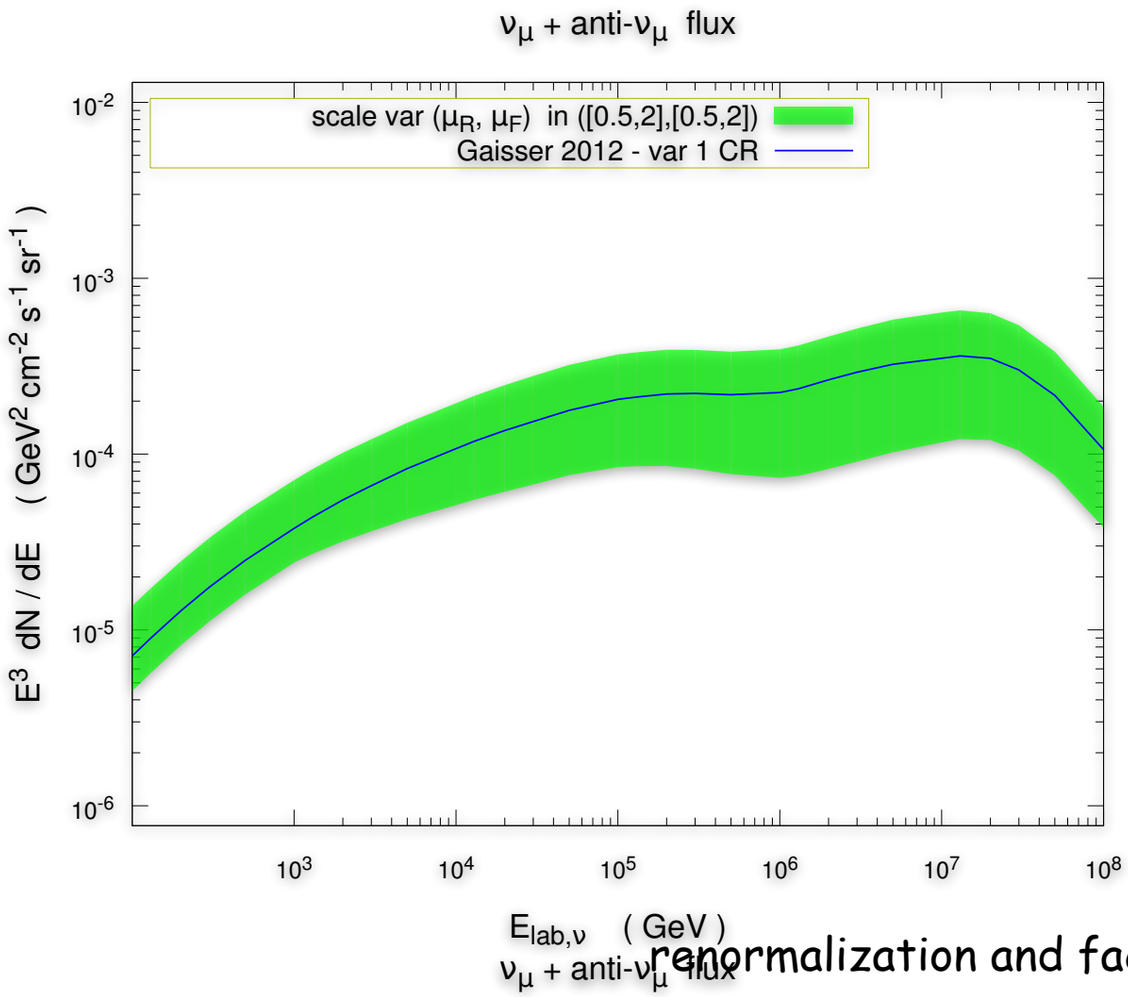

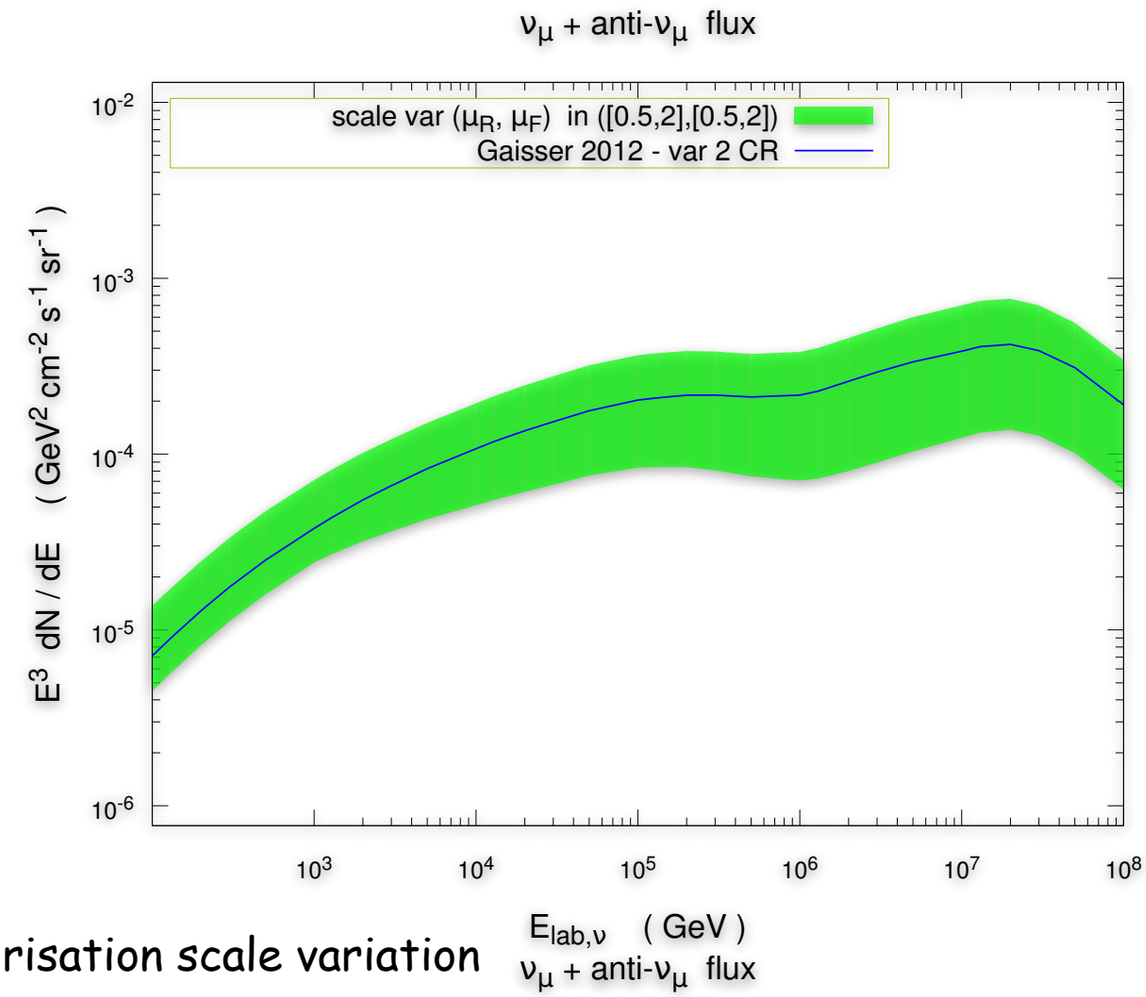

renormalization and factorisation scale variation

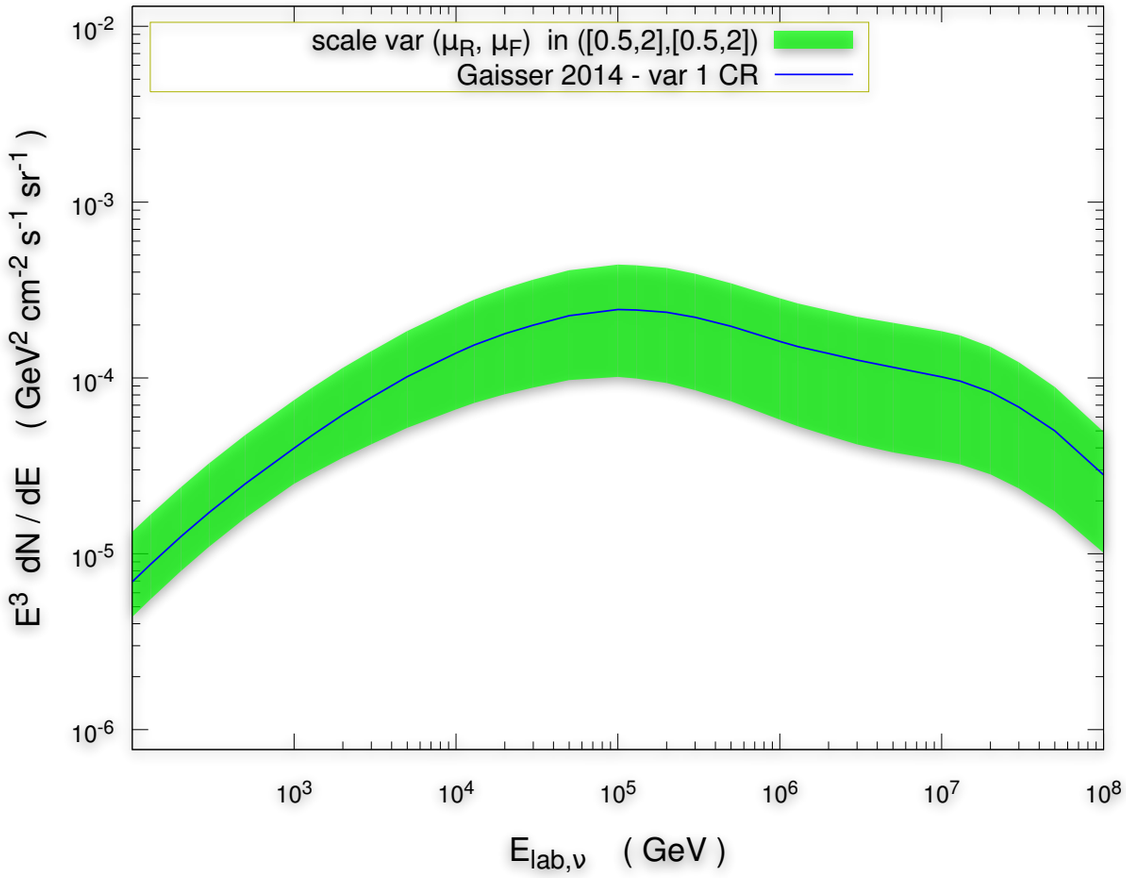

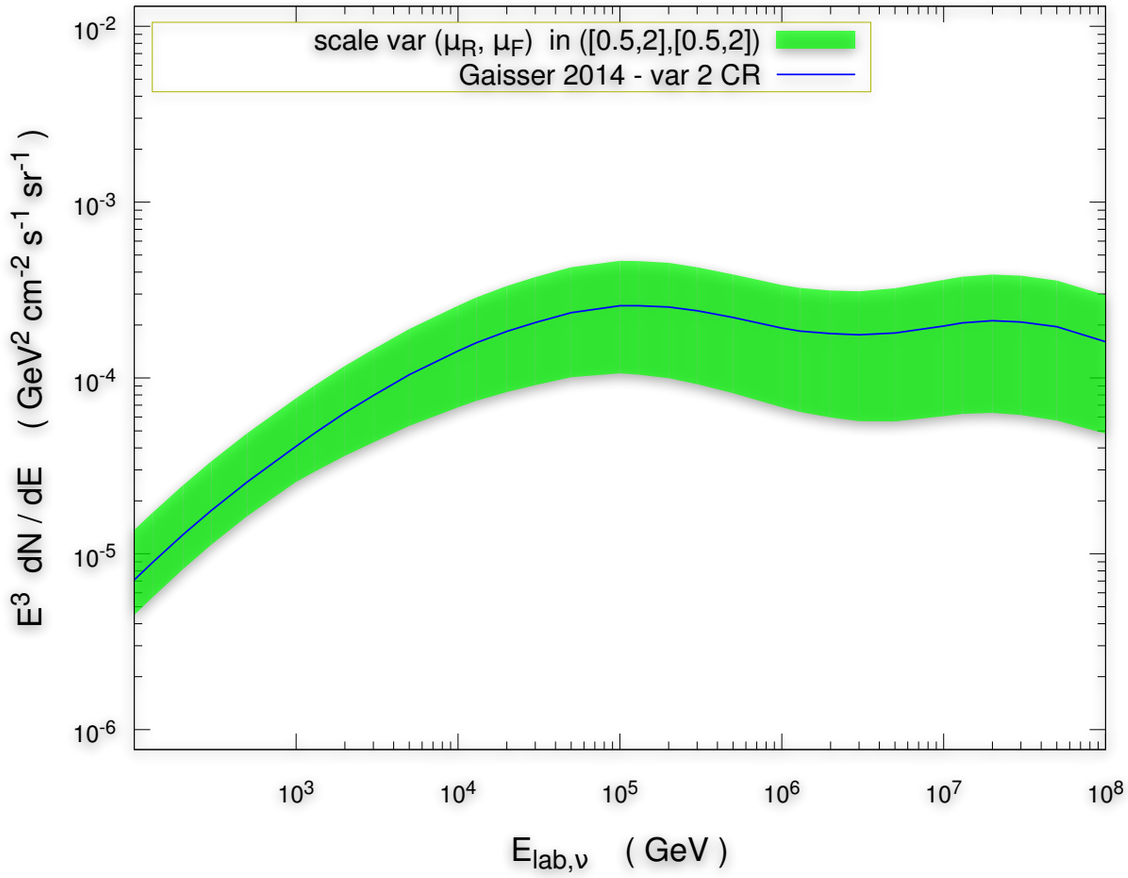

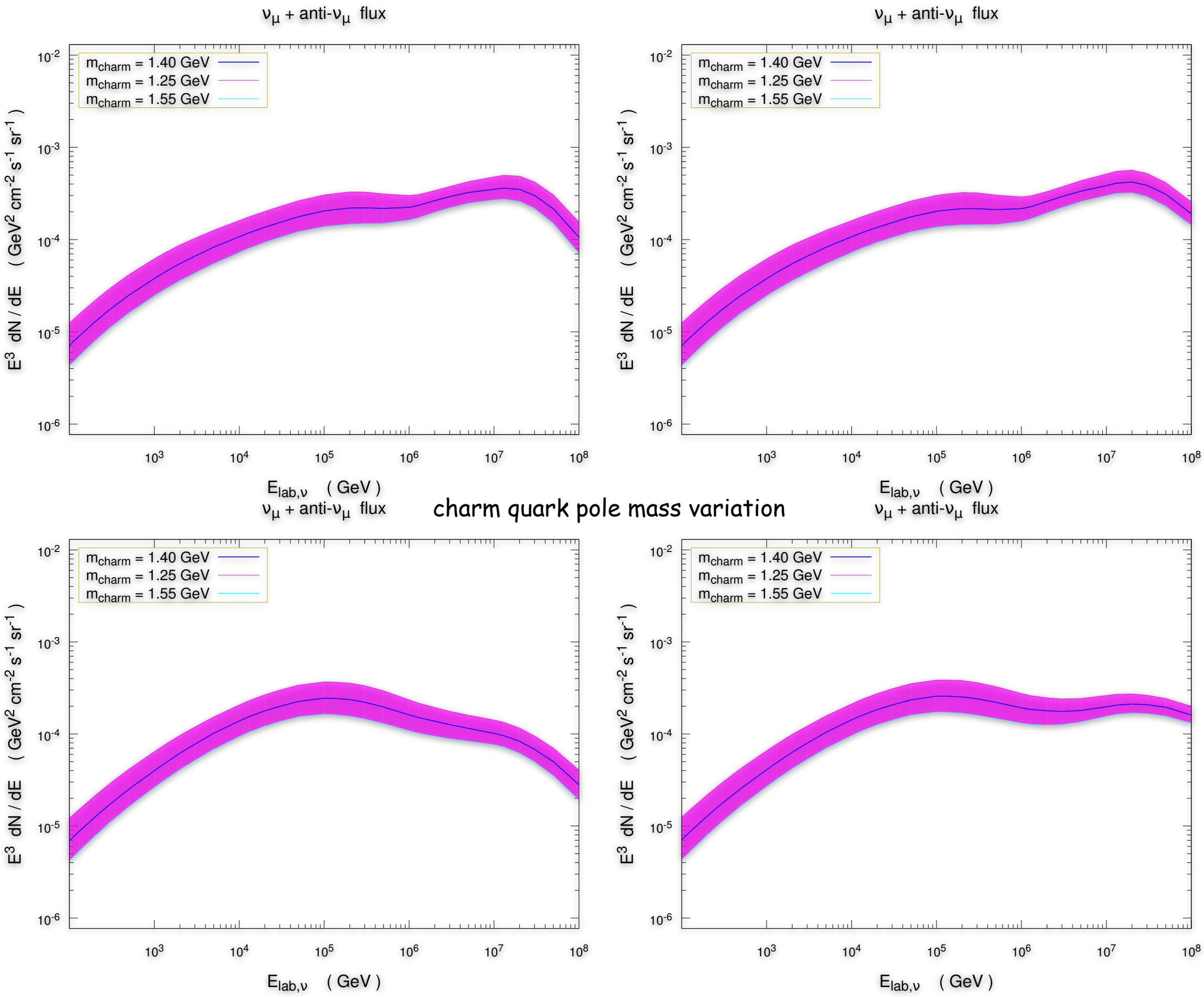
νμ + anti-νμ flux
mcharm = 1.40 GeV
mcharm = 1.25 GeV
mcharm = 1.55 GeV
E3 dN / dE (GeV2 cm-2 s-1 sr-1)
10-2
10-3
10-4
10-5
10-6
10³
10⁴
10⁵
10⁶
10⁷
10⁸
Elab,ν (GeV)
νμ + anti-νμ flux
charm quark pole mass variation
νμ + anti-νμ flux
mcharm = 1.40 GeV
mcharm = 1.25 GeV
mcharm = 1.55 GeV
E3 dN / dE (GeV2 cm-2 s-1 sr-1)
Elab,ν (GeV)
νμ + anti-νμ flux
mcharm = 1.40 GeV
mcharm = 1.25 GeV
mcharm = 1.55 GeV
E3 dN / dE (GeV2 cm-2 s-1 sr-1)
Elab,ν (GeV)
mcharm = 1.40 GeV
mcharm = 1.25 GeV
mcharm = 1.55 GeV
E3 dN / dE (GeV2 cm-2 s-1 sr-1)
Elab,ν (GeV)

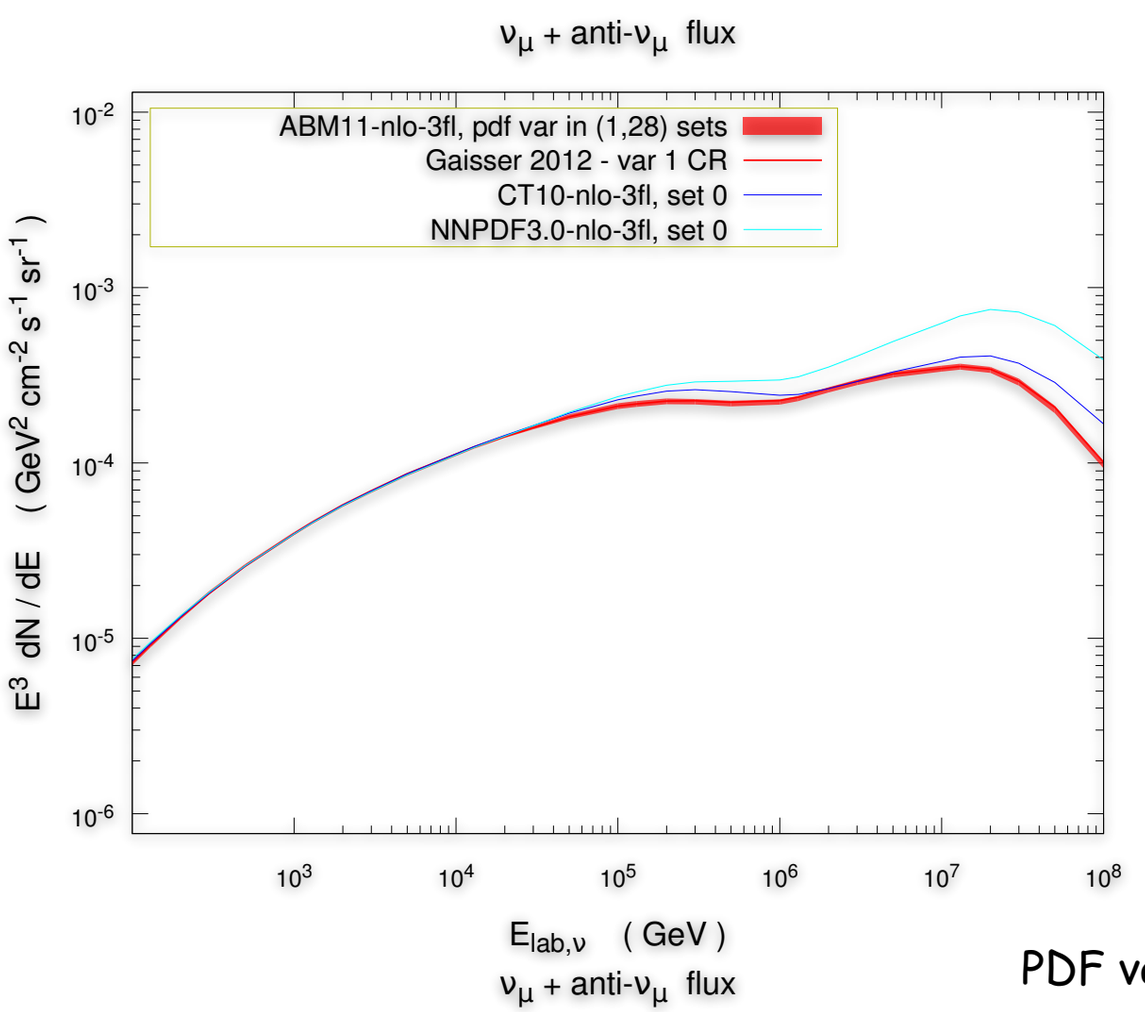

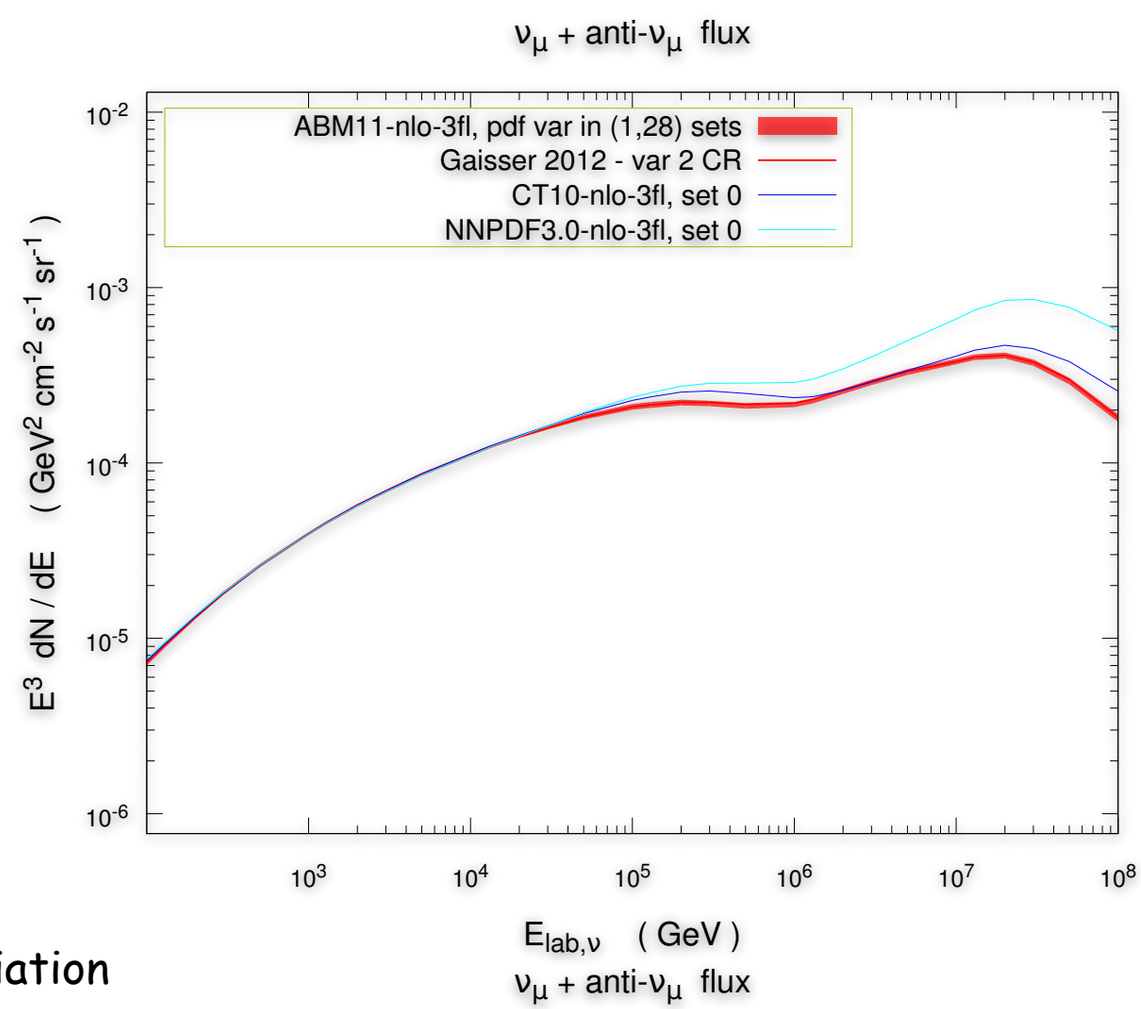

PDF variation

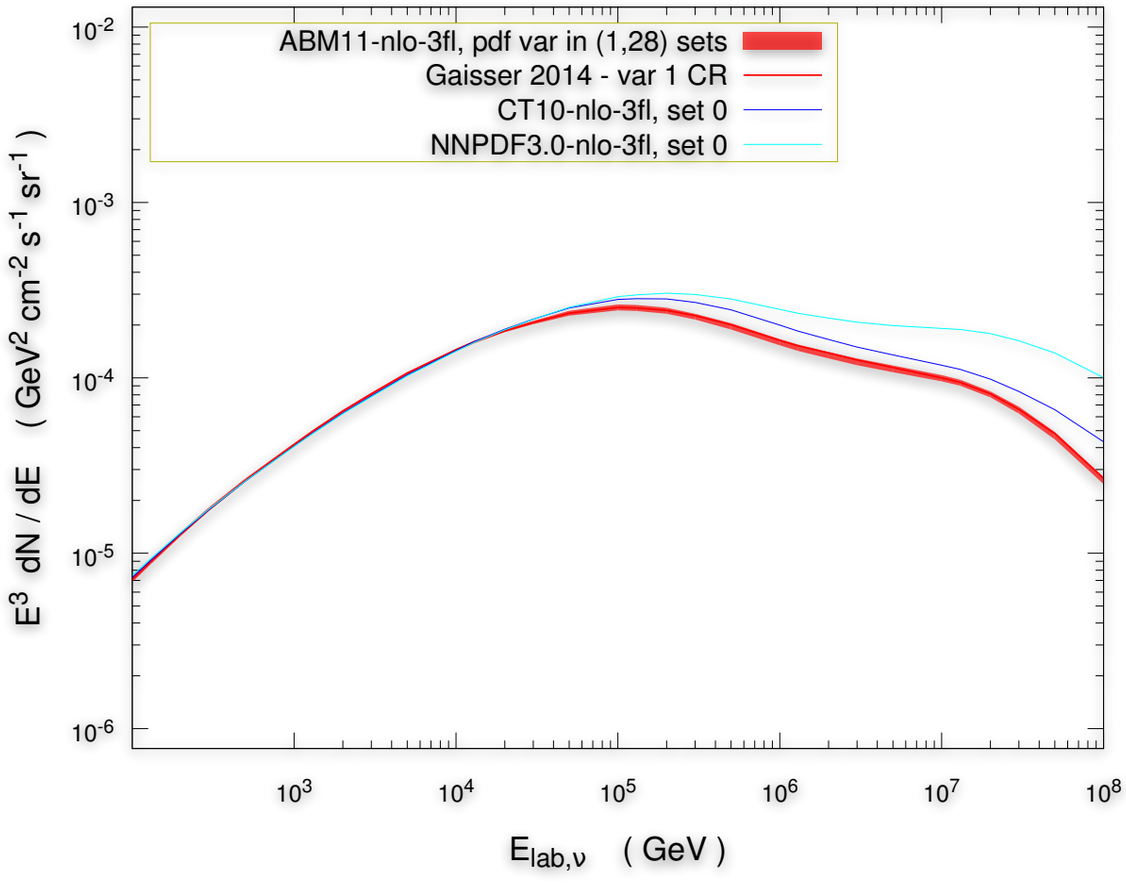

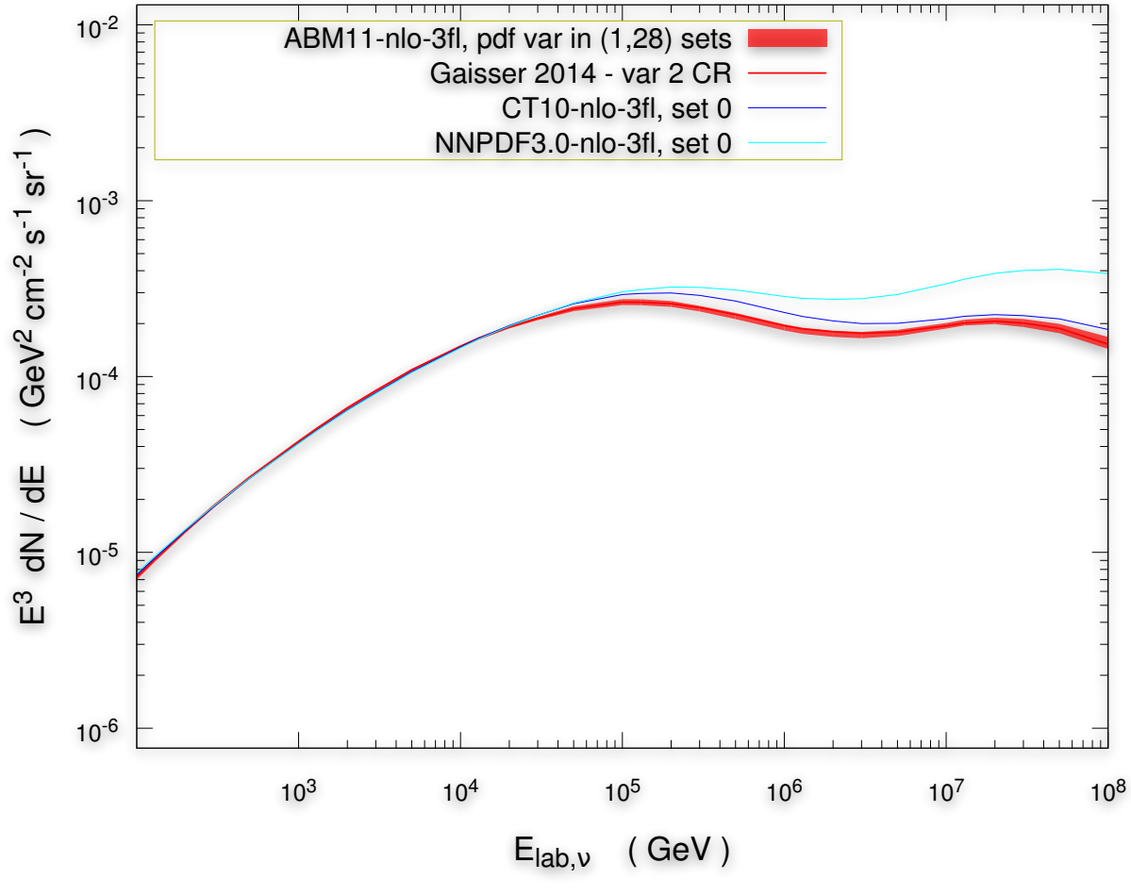

Summary of variations

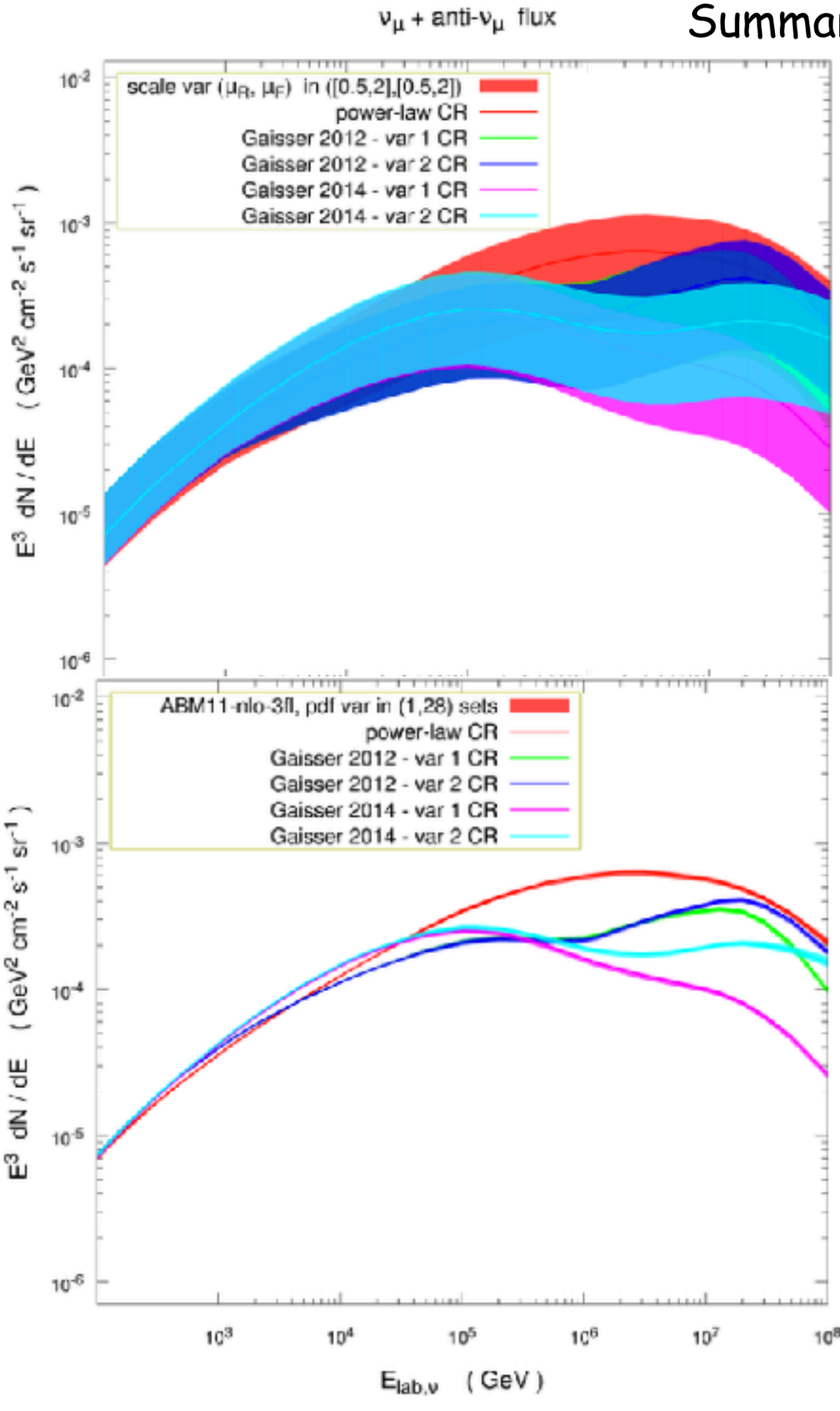

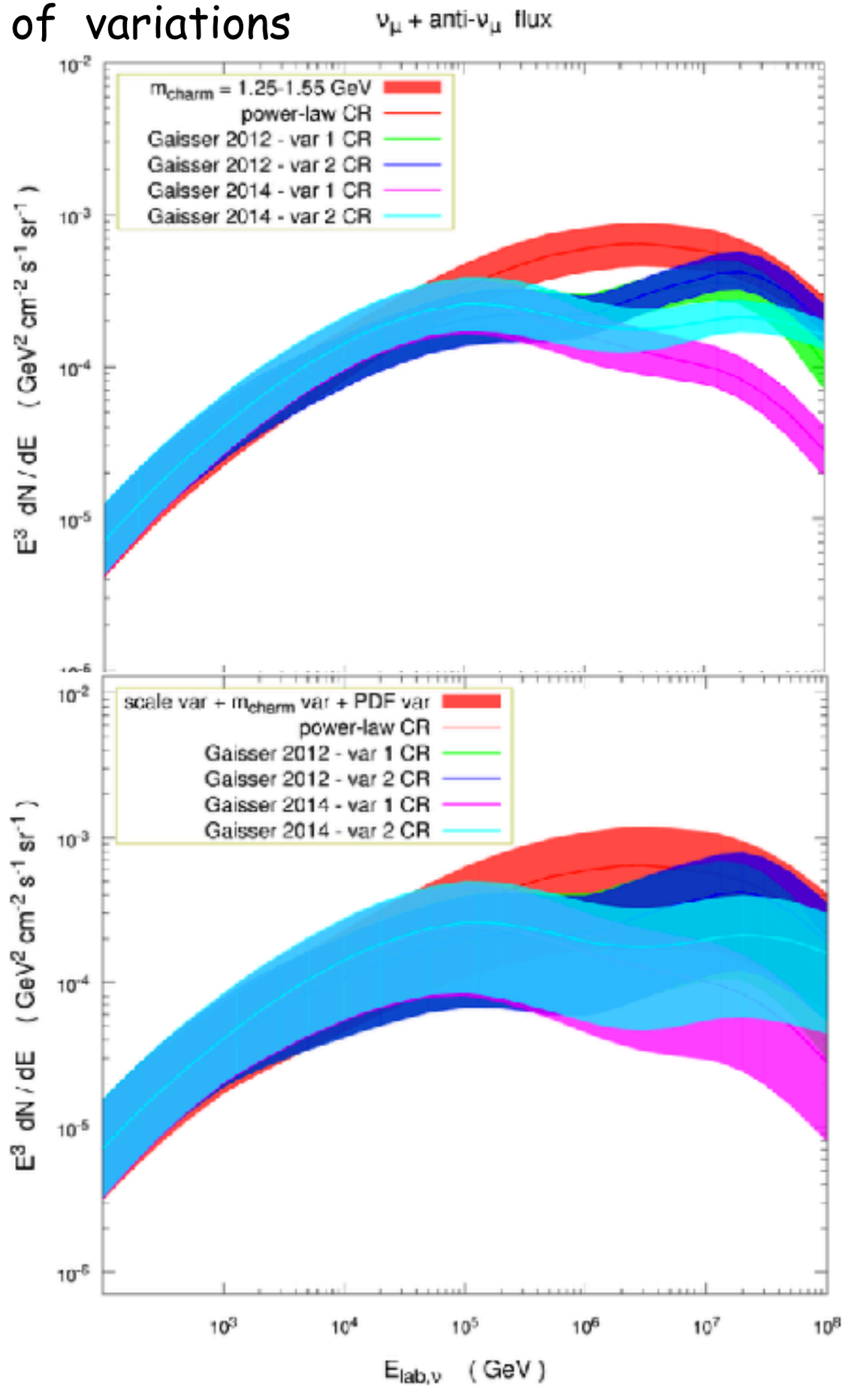

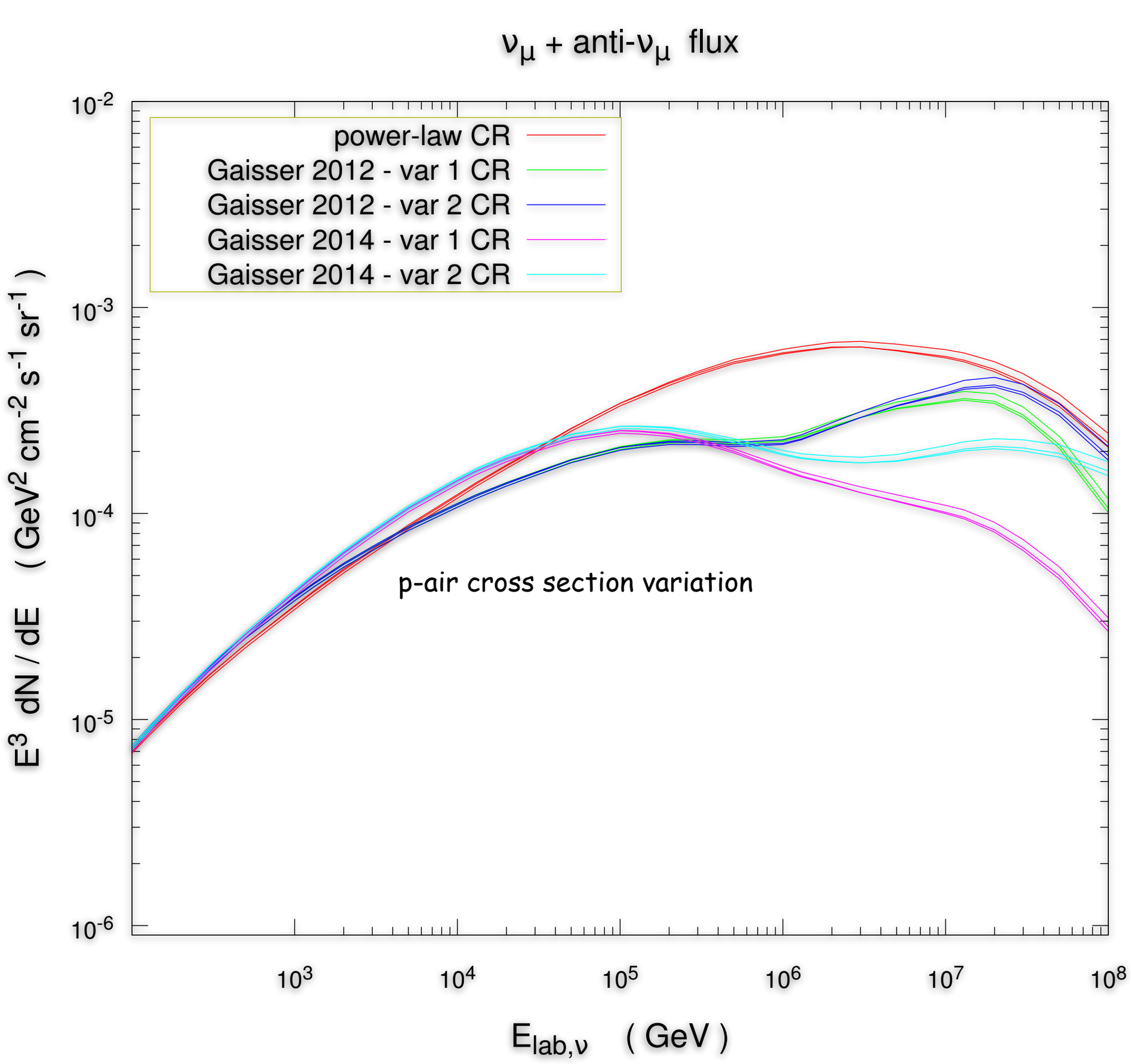
ν_μ + anti-ν_μ flux
power-law CR
Gaisser 2012 - var 1 CR
Gaisser 2012 - var 2 CR
Gaisser 2014 - var 1 CR
Gaisser 2014 - var 2 CR
p-air cross section variation
E^3 dN / dE (GeV^2 cm^{-2} s^{-1} sr^{-1})
$E_{lab,\nu}$ (GeV)
10^{-2}
10^{-3}
10^{-4}
10^{-5}
10^{-6}
10^3
10^4
10^5
10^6
10^7
10^8

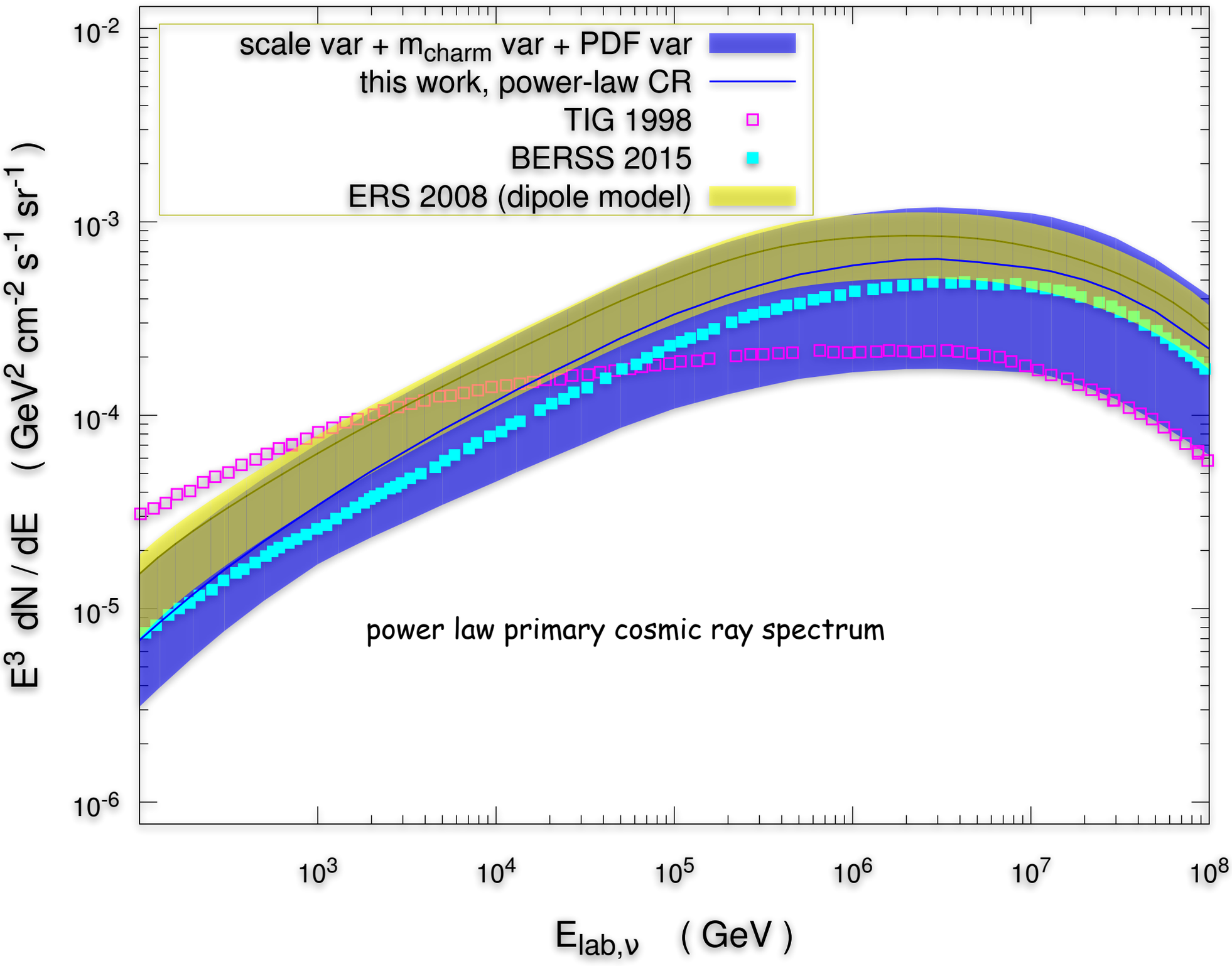
ν_μ + anti-ν_μ flux
scale var + m_{charm} var + PDF var
this work, power-law CR
TIG 1998
BERSS 2015
ERS 2008 (dipole model)
power law primary cosmic ray spectrum
E^3 dN / dE
(GeV^2 cm^{-2} s^{-1} sr^{-1})
10^{-2}
10^{-3}
10^{-4}
10^{-5}
10^{-6}
10^3
10^4
10^5
10^6
10^7
10^8
$E_{lab,\nu}$ (GeV)

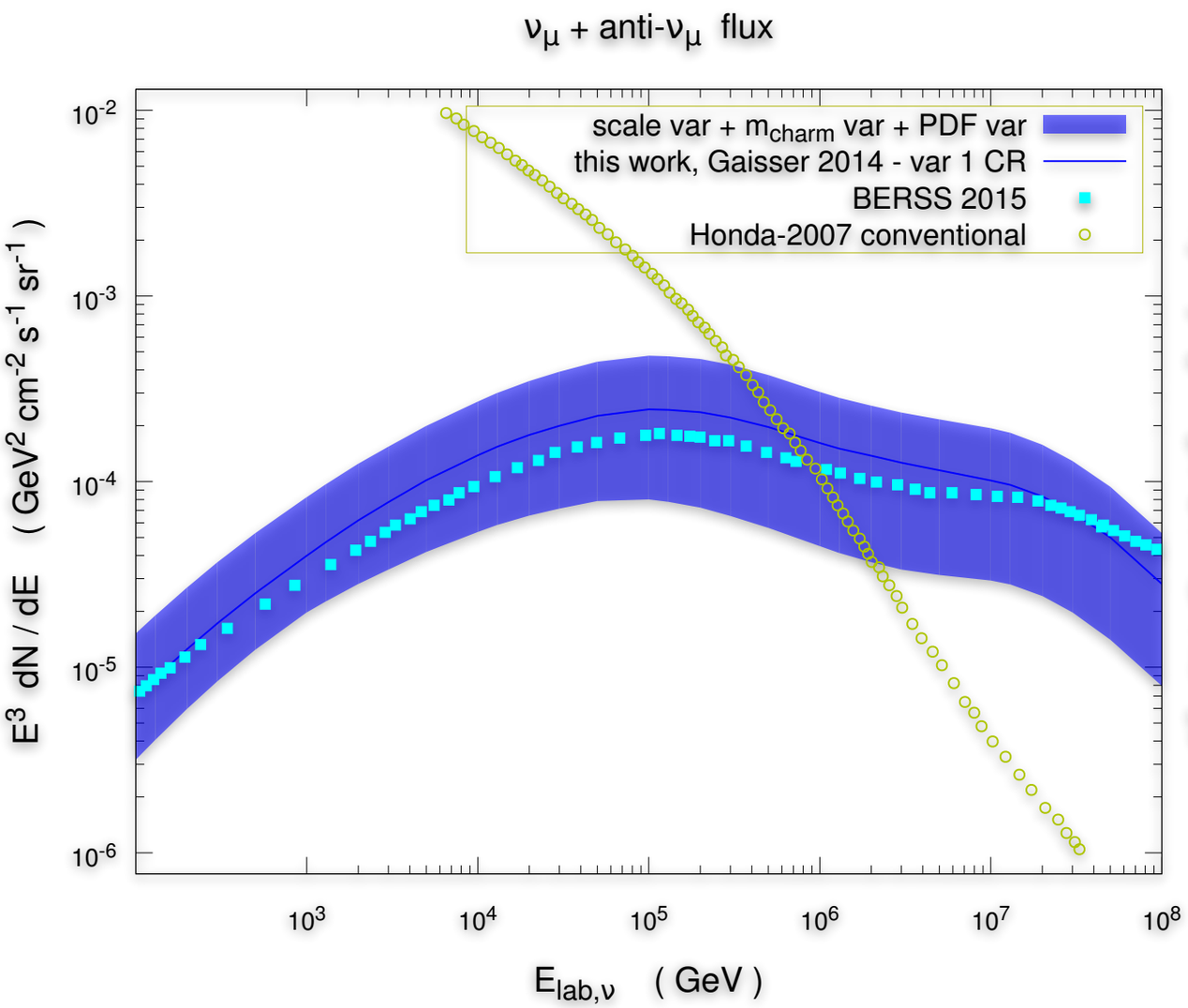

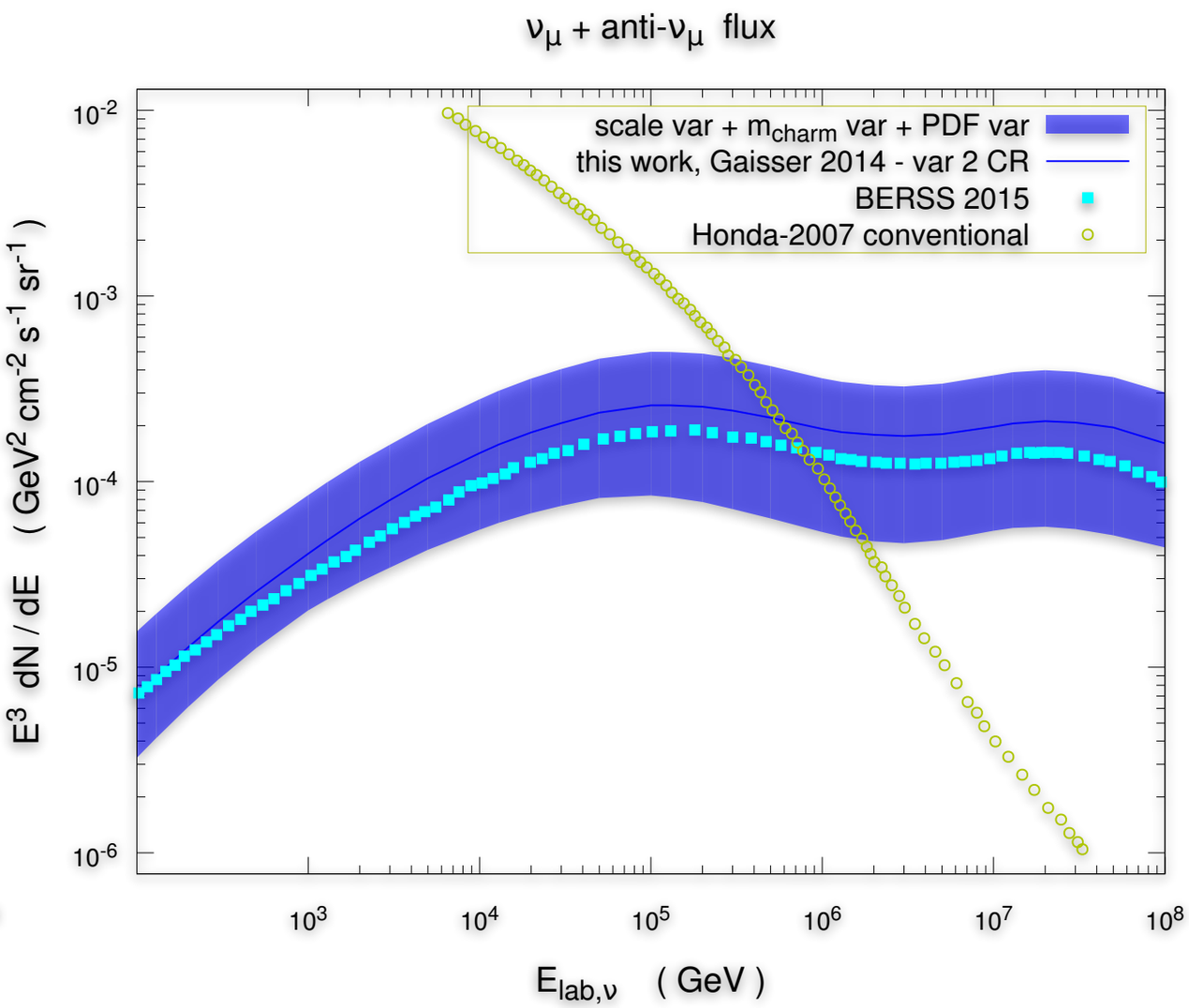

extragalactic mixed (left panel) versus pure proton (right panel) composition, Gaisser 2014

Prompt neutrino fluxes with intrinsic charm

(PRELIMINARY)

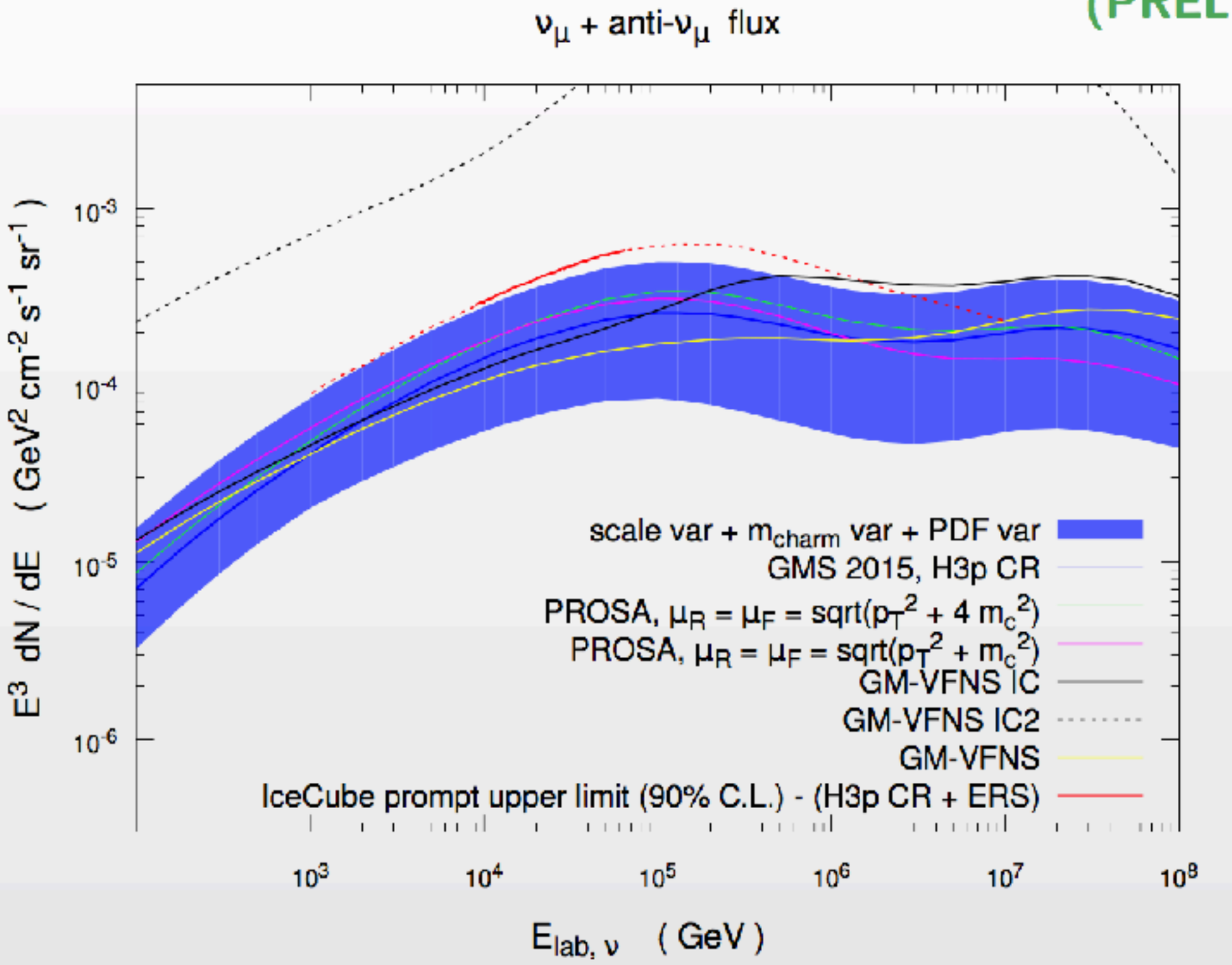

Other calculations:

- Halzen and Wille (upper limit somehow compatible with our IC2)
- Laha and Brodsky (smaller upper limit).

predicted and observed IceCube neutrino fluxes based on PROSA (Proton Structure Analysis in Hadronic Collisions) PDF

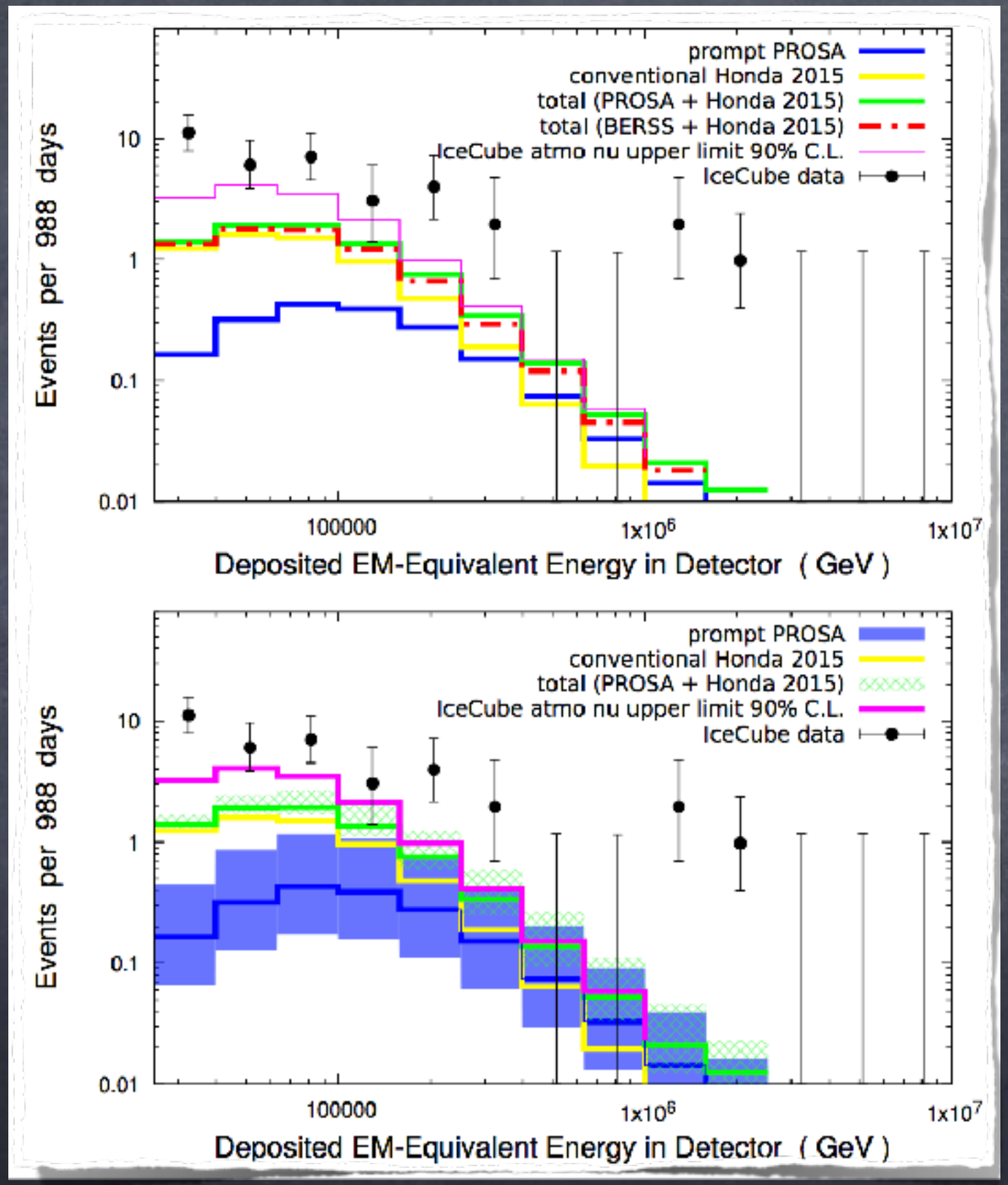

M. Garzelli et al., arXiv:1611.03815

Wish List for Air Shower Physics

1.) use lighter target gases, ideally nitrogen and oxygen

2.) measuring pion, kaon (unflavored meson) and anti-proton production for these cases will be useful to tune Monte Carlo generators

3.) information on nuclear modification factor

4.) information on inclusive heavy flavour production to check the energy dependence of the cross section

5.) ideally, a dedicated forward detector

6.) extend the measurement range to $|\eta|\sim 8\text{-}9$ to close the gap at $6<|\eta|<8$

Conclusions 1

1.) Correct modeling of hadronic interactions is crucial for deducing the cosmic ray mass composition from the data

2.) Air shower data contain a muon excess compared to predictions of current hadronic models

Conclusions 2

1.) Recent updates on prompt neutrino component based on latest QCD results and data, in particular LHCb, are important to interpret HE neutrino fluxes

2.) deduced uncertainties are relatively large, up to a factor ten; dominated by QCD and above ~ 10^6 GeV by cosmic ray total nucleon flux
influence of composition (and flux) uncertainties should be updated and projected as a band

3.) Atmospheric neutrinos are an important background for astrophysical neutrinos for which model and constraint building is now in full gear